Inorg. Chem. **2008**, *47*, 241–256

Carbon Monoxide Coordination and Reversible Photodissociation in Copper(I) Pyridylalkylamine Compounds

H. Christopher Fry, Heather R. Lucas, Amy A. Narducci Sarjeant, Kenneth D. Karlin,* and Gerald J. Meyer*

The Johns Hopkins University, Department of Chemistry, 3400 North Charles Street, Baltimore, Maryland 21218

Received September 25, 2007

Systematic studies of CO coordination and photodissociation have been carried out for a series of copper(I) carbonyl compounds possessing tripodal tetradentate ligands, $[Cu^{I}(L)(CO)]B(C_6F_5)_4$ (L = Me_2N-TMPA (**1**^{Me2N}), MeO-TMPA (**1**^{MeO}), H-TMPA (**1**^{H}), PMEA (**2**^{pmea}), PMAP (**2**^{pmap}), BQPA (**3**^{bqpa}). Detailed structural, electrochemical, and infrared characterization has been accomplished. In addition, various experimental techniques were utilized to determine equilibrium binding constants (K_{CO}), association (k_{CO}), and dissociation (k_{-CO}) rate constants, as well as the thermodynamic ($\Delta H°$, $\Delta S°$) and activation parameters ($\Delta H^{‡}$, $\Delta S^{‡}$) that regulate these processes. With increased ligand-electron-donating ability, greater π back-bonding results in stronger Cu–CO bonds, leading to K_{CO} values on the order **1**^{Me2N}**–CO** > **1**^{MeO}**–CO** > **1**^{H}**–CO**. With systematic synthetic expansion of the five-membered chelate rings like **1**^{R} to six-membered chelate rings like **2**^{R}, the stability of the CO adduct decreases, **1**^{H}**–CO** > **2**^{pmea}**–CO** > **2**^{pmap}**–CO**. The CO-binding properties of **3**^{bqpa} did not follow trends observed for the other compounds, presumably because of its bulkier ligand framework. Through solid- and solution-state analyses, we concluded that the photolabile carbonyl species in solution possess a tridentate coordination mode, forming strictly five-membered chelate rings to the copper ion with one dangling arm of the tripodal ligand. Carbon monoxide reversibly photodissociated from complexes **1**^{Me2N}**–CO**, **1**^{MeO}**–CO**, **1**^{H}**–CO**, and **3**^{bqpa}**–CO** in coordinating (CH_3CN) and weakly coordinating (THF) solvent but not from **2**^{pmea}**–CO** and **2**^{pmap}**–CO**. Comparisons to O_2-binding data available for these copper complexes as well as to small molecule (O_2, CO, NO) reactions with hemes and copper proteins are discussed.

Introduction

Carbon monoxide (CO) and dioxygen (O_2) are known to competitively interact with iron- and copper-ion-containing enzymes. Both ligands have empty π-antibonding orbitals that are available for interactions with filled-metal d orbitals. Copper(I) and its redox partner copper(II) comprise the chemistry involved in copper metalloprotein function, such as electron transfer[1] or the processing of dioxygen (O_2)[2−5] and/or nitrogen oxides.[6] To probe the reduced form of such metalloproteins, CO has been employed as a redox-inactive surrogate for dioxygen, as its readily observable infrared (IR) absorption band(s) can provide insights into the nature of the copper coordination environment, small molecule association/dissociation dynamics, and active-site locale.

Early work involving CO binding to copper proteins such as hemocyanin[7−9] (Hc, arthropodal and molluscan blood O_2-carrier) aided in the description of the dicopper catalytic center as unsymmetrical because of the unequal binding of CO (1 equiv per dicopper). Spectroscopic and chemical similarities to Hc show that the active sites of tyrosinase[10−12] (Tyr, ubiquitous *o*-phenol monooxygenase) and catechol

* To whom correspondence should be addressed. karlin@jhu.edu (K.D.K.), meyer@jhu.edu (G.J.M.).

(1) Rorabacher, D. B. *Chem. Rev.* **2004**, *104*, 651−697.
(2) Quant Hatcher, L.; Karlin, K. D. *J. Biol. Inorg. Chem.* **2004**, *9*, 669−683.
(3) Mirica, L. M.; Ottenwaelder, X.; Stack, T. D. P. *Chem. Rev.* **2004**, *104*, 1013−1045.
(4) Lewis, E. A.; Tolman, W. B. *Chem. Rev.* **2004**, *104*, 1047−1076.
(5) Lee, Y.; Karlin, K. D. In *Concepts and Models in Bioinorganic Chemistry*; Metzler-Nolte, N., Kraatz, H.-B., Eds.; Wiley-VCH: New York, 2006; pp 363−395.
(6) Wasser, I. M.; de Vries, S.; Moënne-Loccoz, P.; Schröder, I.; Karlin, K. D. *Chem. Rev.* **2002**, *102*, 1201−1234.
(7) Bonaventura, C.; Sullivan, B.; Bonaventura, J.; Bourne, S. *Biochemistry* **1974**, *13*, 4784−4789.
(8) Sorrell, T. N.; Jameson, D. L. *J. Am. Chem. Soc.* **1982**, *104*, 2053−2054.
(9) Ellerton, H. D.; Ellerton, N. F.; Robinson, H. A. *Prog. Biophys. Mol. Biol.* **1983**, *41*, 143−248.

10.1021/ic701903h CCC: $40.75
Published on Web 12/04/2007

oxidase[13−15] are also asymmetric. More recently, stoichiometric CO binding studies and IR spectroscopic measurements helped to characterize the structural and functional inequivalence of the two copper(I) centers ($Cu_A \equiv Cu_H$, $Cu_B \equiv Cu_M$) of reduced dopamine-β-monoxygenase (DβH)[16−18] and peptidylglycine monooxygenase (PHM).[19−22] In addition, CO facilitated the characterization/description of an unprecedented S-donor methionine ligand at the Cu_B/Cu_M site and aided in the elucidation of the ligand environment for the Cu^I versus Cu^{II} centers.

Although CO has been most commonly utilized to determine active site structure in copper enzymes, it has also helped in elucidating mechanistic pathways. For example, the ability of CO to bind to both PHM metal sites, surprisingly even Cu_H when peptidylglycine substrates bind,[22] at the time led to new hypotheses for probing the enzyme mechanism and dynamics (i.e., superoxide channeling[20,22] vs hydrogen tunneling for the substrate hydrogen atom abstraction[23−27]) of the uncoupled metal centers. In addition, the course of CO and presumably O_2 reactivity in the heme$_{a3}$/Cu_B active site of cytochrome *c* oxidase (C*c*O) has been probed through laser flash photolysis (LFP).[28−33] Upon the photorelease of carbon monoxide from heme$_{a3}$, CO rapidly (ps) moves to Cu^I_B and subsequently escapes or returns to the heme$_{a3}$ on a millisecond time-scale, suggesting that Cu^I_B can act as a doorway for substrate O_2-binding to heme$_{a3}$ in this binuclear active site of C*c*O. LFP is a common methodology used to probe heme protein-actives-site environments giving kinetic and thermodynamic insights.[33−35]

Chart 1

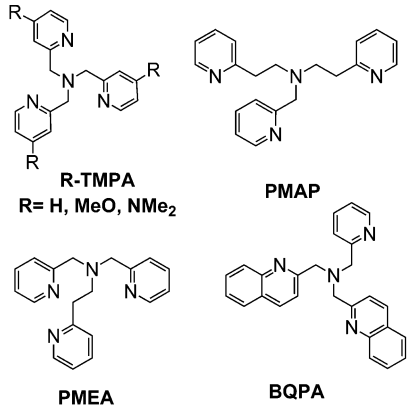

$\mathbf{1^{Me_2N}}$	$[Cu^I(Me_2N\text{-tmpa})]^+$	$\mathbf{1^{Me_2N}\text{-}CO}$	$[Cu^I(Me_2N\text{-tmpa})(CO)]^+$
$\mathbf{1^{MeO}}$	$[Cu^I(MeO\text{-tmpa})(CH_3CN)]^+$	$\mathbf{1^{MeO}\text{-}CO}$	$[Cu^I(MeO\text{-tmpa})(CO)]^+$
$\mathbf{1^{H}}$	$[Cu^I(H\text{-tmpa})(CH_3CN)]^+$	$\mathbf{1^{H}\text{-}CO}$	$[Cu^I(H\text{-tmpa})(CO)]^+$
$\mathbf{2^{pmea}}$	$[Cu^I(pmea)]^+$	$\mathbf{2^{pmea}\text{-}CO}$	$[Cu^I(pmea)(CO)]^+$
$\mathbf{2^{pmap}}$	$[Cu^I(pmap)]^+$	$\mathbf{2^{pmap}\text{-}CO}$	$[Cu^I(pmap)(CO)]^+$
$\mathbf{3^{bqpa}}$	$[Cu^I(bqpa)]^+$	$\mathbf{3^{bqpa}\text{-}CO}$	$[Cu^I(bqpa)(CO)]^+$

Whereas CO photoejection has yet to be observed from a protein that has only copper as the active-site metal, we recently communicated that metal-to-ligand charge-transfer (MLCT) excitation of at least one type of copper(I) carbonyl complex, $[Cu^I(H\text{-tmpa})(CO)]^+$ (**1^H−CO**; TMPA = tris(2-pyridylmethyl)amine); Chart 1), resulted in the efficient release of CO.[36] The CO rebinding was quantitative, and no net photochemistry was observed. The rate constant for CO rebinding following flash photolysis of **1^H−CO** in tetrahydrofuran solvent (THF) was determined to approach a diffusion-controlled value, $k_{CO} = 1.9 \times 10^9\ M^{-1}\ s^{-1}$ at 25 °C. We were also successful at applying the flash-and-trap technique, pioneered by Gibson and co-workers for heme protein analysis.[37] Light excitation ($\lambda_{ex} = 355$ nm) of **1^H−CO** in the presence of O_2 in THF resulted in the transient appearance of a primary copper(I)−dioxygen adduct, a cupric−superoxo ($Cu^{II}(O_2^{\bullet -})$) species.[38] The temperature dependence of this rate constant implied a value of $k_{O2} = 1.3 \times 10^9\ M^{-1}\ s^{-1}$ at 25 °C. Remarkably, this rate constant for dioxygen binding was found to exceed that previously measured for synthetic or biological hemes.[35,39−41] Of even greater significance are the nearly equal k_{CO} and k_{O2} values

(10) Solomon, E. I.; Sundaram, U. M.; Machonkin, T. E. *Chem. Rev.* **1996**, *96*, 2563−2605.
(11) DellaLonga, S.; Ascone, I.; Bianconi, A.; Bonfigli, A.; Castellano, A. C.; Zarivi, O.; Miranda, M. *J. Biol. Chem.* **1996**, *271*, 21025−21030.
(12) Matoba, Y.; Kumagai, T.; Yamamoto, A.; Yoshitsu, H.; Sugiyama, M. *J. Biol. Chem.* **2006**, *281*, 8981−8990.
(13) Klabunde, T.; Eicken, C.; Sacchettini, J. C.; Krebs, B. *Nature Struct. Biol.* **1998**, *5*, 1084−1090.
(14) Rompel, A.; Fischer, H.; Meiwes, D.; Buldt-Karentzopoulos, K.; Dillinger, R.; Tuczek, F.; Witzel, H.; Krebs, B. *J. Biol. Inorg. Chem.* **1999**, *4*, 56−63.
(15) Gerdemann, C.; Eicken, C.; Krebs, B. *Acc. Chem. Res.* **2002**, *35*, 183−191.
(16) Blackburn, N. J.; Pettingill, T. M.; Seagraves, K. S.; Shigeta, R. T. *J. Biol. Chem.* **1990**, *265*, 15383−15386.
(17) Pettingill, T. M.; Strange, R. W.; Blackburn, N. J. *J. Biol. Chem.* **1991**, *266*, 16996−17003.
(18) Reedy, B. J.; Blackburn, N. J. *J. Am. Chem. Soc.* **1994**, *116*, 1924−1931.
(19) Boswell, J. S.; Reedy, B. J.; Kulathila, R.; Merkler, D.; Blackburn, N. J. *Biochemistry* **1996**, *35*, 12241−12250.
(20) Jaron, S.; Blackburn, N. J. *Biochemistry* **1999**, *38*, 15086−15096.
(21) Jaron, S.; Blackburn, N. J. *Biochemistry* **2001**, *40*, 6867−6875.
(22) Jaron, S.; Mains, R. E.; Eipper, B. A.; Blackburn, N. J. *Biochemistry* **2002**, *41*, 13274−13282.
(23) Francisco, W. A.; Knapp, M. J.; Blackburn, N. J.; Klinman, J. P. *J. Am. Chem. Soc.* **2002**, *124*, 8194−8195.
(24) Chen, P.; Solomon, E. I. *J. Am Chem. Soc.* **2004**, *126*, 4991−5000.
(25) Bauman, A. T.; Jaron, S.; Yukl, E. T.; Burchfiel, J. R.; Blackburn, N. J. *Biochemistry* **2006**, *45*, 11140−11150.
(26) Bauman, A. T.; Yukl, E. T.; Alkevich, K.; McCormack, A. L.; Blackburn, N. J. *J. Biol. Chem.* **2006**, *281*, 4190−4198.
(27) Klinman, J. P. *J. Biol. Chem.* **2006**, *281*, 3013−3016.
(28) Alben, J. O.; Moh, P. P.; Fiamingo, F. G.; Altschuld, R. A. *Proc. Natl. Acad. Sci-Biol.* **1981**, *78*, 234−237.
(29) Einarsdottir, O.; Dyer, R. B.; Lemon, D. D.; Killough, P. M.; Hubig, S. M.; Atherton, S. J.; Lopez-Garriga, J. J.; Palmer, G.; Woodruff, W. H. *Biochemistry* **1993**, *32*, 12013−24.
(30) Stavrakis, S.; Koutsoupakis, K.; Pinakoulaki, E.; Urbani, A.; Saraste, M.; Varotsis, C. *J. Am Chem. Soc.* **2002**, *124*, 3814−3815.
(31) Okuno, D.; Iwase, T.; Shinzawa-Itoh, K.; Yoshikawa, S.; Kitagawa, T. *J. Am. Chem. Soc.* **2003**, *125*, 7209−7218.
(32) McMahon, B. H.; Fabian, M.; Tomson, F.; Causgrove, T. P.; Bailey, J. A.; Rein, F. N.; Dyer, R. B.; Palmer, G.; Gennis, R. B.; Woodruff, W. H. *Bba-Bioenergetics* **2004**, *1655*, 321−331.
(33) Larsen, R. W.; Miksovska, J. *Coord. Chem. Rev.* **2007**, *251*, 1101−1127.
(34) Niederhoffer, E. C.; Timmons, J. H.; Martell, A. E. *Chem. Rev.* **1984**, *84*, 137.
(35) Momenteau, M.; Reed, C. A. *Chem. Rev.* **1994**, *94*, 659−698.
(36) Scaltrito, D. V.; Fry, H. C.; Showalter, B. M.; Thompson, D. W.; Liang, H.-C.; Zhang, C. X.; Kretzer, R. M.; Kim, E.-i.; Toscano, J. P.; Karlin, K. D.; Meyer, G. J. *Inorg. Chem.* **2001**, *40*, 4514−4515, and refs cited therein.
(37) Greenwood, C.; Gibson, Q. H. *J. Biol. Chem.* **1967**, *242*, 1782−1787.
(38) Fry, H. C.; Scaltrito, D. V.; Karlin, K. D.; Meyer, G. J. *J. Am Chem. Soc.* **2003**, *125*, 11866−11871.
(39) Collman, J. P.; Boulatov, R.; Sunderland, C. J.; Fu, L. *Chem. Rev.* **2004**, *104*, 561−588.
(40) Collman, J. P.; Brauman, J. I.; Doxsee, K. M.; Sessler, J. L.; Morris, R. M.; Gibson, Q. H. *Inorg. Chem.* **1983**, *22*, 1427−1432.

Scheme 1

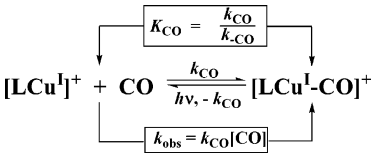

as has been observed in other copper proteins and heme systems (vide infra).

Thus, CO appears as an excellent surrogate for O_2, and further elucidation of the dynamics of CO binding to copper(I) complexes is of bioinorganic relevance. The ability to probe the ligand environment and function relevant to copper protein-actives sites is an area of great interest because it is already established that the detailed nature of the ligand environment around copper (i.e., donor atom type, number of donors, coordination geometry, etc.) dictates the course of (ligand)Cu^I/O_2 chemistry, dynamics, dioxygen coordination mode, and subsequent reactivity toward substrates.[2−4] Here, we report systematic studies of CO coordination and photodissociation for a series of copper(I) compounds possessing tripodal tetradentate ligand analogues of TMPA. The studies are designed to test generality and to determine some rules for the realization of this novel photochemistry. To probe electronic effects, the pyridyl donors of the parent TMPA ligand have been *para*-substituted with electron-donating $-NMe_2$ or $-OMe$ substituents (**1^R**, Chart 1).[42] In addition, the ligand chelate ring size has been systematically increased by employing the ligand series **2^R**, PMEA → PMAP → TEPA (Chart 1).[43] Finally, a bulkier and more hydrophobic ligand, BQPA, contains one pyridyl and two quinolyl arms (Chart 1).[44] The choice of these ligands comes in part from their previous use in (ligand)−copper(I)/O_2 reactivity studies.[42−44]

Microsecond fast CO-binding rates like those reported here can only be obtained using flash photolytic techniques; other methods such as stopped-flow do not offer a sufficient time resolution. Therefore, the literature involving LCu^I−CO kinetics has been very limited and the thermodynamics ($\Delta H^{\ddagger}$, $\Delta S^{\ddagger}$) that govern these dynamics are nonexistent (as far as we have investigated). Here, we present the first such detailed investigation of CO and copper(I) interactions. In addition to new transient absorption laser flash-photolysis CO-recombination kinetic studies, we also present here complementary chemical investigations (Scheme 1). Detailed structural, electrochemical, infrared, and equilibrium CO-binding studies (via UV−vis spectrophotometric titrations) have been carried out. Comparisons to data available for O_2 binding to these copper complexes as well as to small-molecule (i.e., O_2, CO or NO) reactions with hemes and copper proteins are discussed.

Experimental Section

Materials and Methods. All of the reagents were purchased from commercial sources. All of the air-sensitive compounds were synthesized utilizing Schlenk techniques. Diethyl ether (Fisher Scientific 99+ %) and tetrahydrofuran (THF; EMD 99%) solvents were purified by passing through a series of activated alumina columns (Innovative Technology; Newburyport, MA). Acetonitrile (CH_3CN, Fisher Scientific 99+ %) was dried and distilled over calcium hydride under an argon (Air Gas East, grade 4.8) atmosphere. The solvents CH_3CN and THF were introduced into an MBraun Labmaster 130 dry box (O_2 < 1 ppm; H_2O < 1 ppm) after purging for 1 h with argon gas and then placed under vacuum. Elemental analyses were performed by Desert Analytics (Tucson, AZ) or Quantitative Technologies, Inc. (QTI; Whitehouse, NJ). ^{1}H NMR spectra were recorded at 400 MHz on a Bruker Avance FT-NMR spectrometer. Deuterated nitromethane (CD_3NO_2) was purchased from Aldrich (99%) and deaerated under nitrogen gas (Air Gas East, grade 4.8).

Synthesis. Me_2N-TMPA,[42] MeO-TMPA,[42] H-TMPA,[45] PMEA,[43] PMAP,[43] BQPA,[44] $[Cu^I(CH_3CN)_4]B(C_6F_5)_4$,[46] $[Cu^I(Me_2N\text{-tmpa})]B(C_6F_5)_4$ **(1^{Me2N})**,[42] $[Cu^I(MeO\text{-tmpa})(CH_3CN)]B(C_6F_5)_4$ **(1^{MeO})**,[42] and $[Cu^I(H\text{-tmpa})(CH_3CN)]B(C_6F_5)_4$ **(1^{H})**[42] were prepared according to published procedures.

$[Cu^I(NMe_2\text{-TMPA})(CO)]B(C_6F_5)_4$ (1^{Me2N}-CO). In a 100 mL Schlenk flask equipped with a stir bar, NMe_2-TMPA (34 mg, 0.081 mmol) and $[Cu^I(CH_3CN)_4]B(C_6F_5)_4$ (71 mg, 0.078 mmol) were added together. To this mixture, CO-saturated diethyl ether (5 mL) was added under an atmosphere of CO. The resulting pale-yellow solution was stirred for 75 min while CO was purged through 100 mL of heptane. The CO-saturated heptane was subsequently added to the stirring solution, resulting in a white cloudy mixture. After 2 h of stirring under a CO atmosphere, a white solid precipitated. Additional time was provided for the white powder to settle. The supernatant was removed via a cannula, and the resulting white powder was placed in vacuo for 15 min, yielding 72 mg (77%). Anal. Calcd: C, 49.45; H, 2.79; N, 8.24. Found: C, 49.14; H, 2.66; N, 8.14. ^{1}H NMR (CD_3NO_2): δ 8.68 (3H, s, br), 7.89 (3H, s, br), 7.44 (6H, s, br), 4.15 (6H, s).

$[Cu^I(tmpa)(CO)]B(C_6F_5)_4$ (1^{H}−CO). In a 100 mL Schlenk flask equipped with a stir bar, TMPA (32 mg, 0.11 mmol) and $[Cu^I(CH_3CN)_4]B(C_6F_5)_4$ (100 mg, 0.11 mmol) were added together. To this, CO saturated Et_2O (5 mL) was added under a CO atmosphere. The resulting light-yellow solution was stirred for 30 min. CO-saturated heptane (100 mL) was added to the solution to precipitate the product. After stirring for 1 h, a white solid precipitated. The supernatant was decanted, and the solid was placed in vacuo, yielding 93 mg (80%) of a white powder. Anal. Calcd: C, 48.68; H, 1.71; N, 5.28. Found: C, 48.50; H, 1.89; N, 4.49. ^{1}H NMR (CD_3NO_2): δ 8.68 (3H, s, br), 7.89 (3H, s, br), 7.44 (6H, s, br), 4.15 (6H, s).

$[Cu^I(pmea)]B(C_6F_5)_4$ (2^{pmea}). $[Cu^I(CH_3CN)_4]B(C_6F_5)_4$ (300 mg, 0.33 mmol) was placed in a 100 mL Schlenk flask equipped with a stir. To this solid, PMEA (111 mg, 0.36 mmol) dissolved in dried and deaerated diethyl ether was added under an argon atmosphere. The resulting yellow solution was stirred for 30 min. Dried and

(41) Kano, K.; Kitagishi, H.; Dagallier, C.; Kodera, M.; Matsuo, T.; Hayashi, T.; Hisaeda, Y.; Hirota, S. *Inorg. Chem.* **2006**, *45*, 4448−4460.
(42) Zhang, C. X.; Kaderli, S.; Costas, M.; Kim, E.-i.; Neuhold, Y.-M.; Karlin, K. D.; Zuberbühler, A. D. *Inorg. Chem.* **2003**, *42*, 1807−1824.
(43) Schatz, M.; Becker, M.; Thaler, F.; Hampel, F.; Schindler, S.; Jacobson, R. R.; Tyeklár, Z.; Murthy, N. N.; Ghosh, P.; Chen, Q.; Zubieta, J.; Karlin, K. D. *Inorg. Chem.* **2001**, *40*, 2312−2322.
(44) Wei, N.; Murthy, N. N.; Chen, Q.; Zubieta, J.; Karlin, K. D. *Inorg. Chem.* **1994**, *33*, 1953−1965.
(45) Tyeklár, Z.; Jacobson, R. R.; Wei, N.; Murthy, N. N.; Zubieta, J.; Karlin, K. D. *J. Am. Chem. Soc.* **1993**, *115*, 2677−2689.
(46) Liang, H.-C.; Kim, E.; Incarvito, C. D.; Rheingold, A. L.; Karlin, K. D. *Inorg. Chem.* **2002**, *41*, 2209−2212.

deaerted heptane (100 mL) was added to precipitate the complex. After stirring for 1 h, the supernatant was decanted. The remaining yellow-oily solid was dissolved again in dried and dearated diethyl ether (10 mL) and precipitated with deaerated heptane (100 mL). The resulting solid was placed in vacuo to yield 268 mg (77%) of a yellow powder. Anal. Calcd: C, 49.33; H, 1.93; N, 5.35. Found: C, 49.54; H, 2.21; N, 5.12. ^{1}H NMR (CD_3NO_2): δ 8.93 (br, 3 H), 7.81 (m, br, 3 H), 7.37 (m, br, 6 H), 4.05 (br, 4 H), 3.21 (br, 2 H), 3.01 (br, 2 H).

$[Cu^I(pmap)]B(C_6F_5)_4$ (2^{pmap}). $[Cu(CH_3CN)_4]B(C_6F_5)_4$ (200 mg, 0.22 mmol) was placed in a 100 mL Schlenk flask equipped with a stir bar. To this, PMAP (70 mg, 0.22 mmol) dissolved in dried and deaerated diethyl ether (5 mL) was added under an argon atmosphere. The resulting yellow solution was stirred for 30 min. Deaerted heptane (100 mL) was added to precipitate the complex. After stirring for 1 h, the supernatant was decanted. The resulting solid was placed in vacuo to yield 173 mg (74%) of a yellow powder. Anal. Calcd: C, 49.81; H, 2.09; N, 5.28. Found: C, 49.90; H, 2.36; N, 5.25. ^{1}H NMR (CD_3NO_2): δ 8.84 (m, 3 H), 7.79 (m, 3 H), 7.35 (m, 6 H), 4.28 (s, 2 H), 3.17 (br, 4 H), 2.96 (br, 4 H).

$[Cu^I(bqpa)]B(C_6F_5)_4$ (3^{bqpa}). In a 100 mL Schlenk flask equipped with a stir bar, BQPA (29 mg, 0.074 mmol) and $[Cu(CH_3CN)_4]B(C_6F_5)_4$ (65 mg, 0.071 mmol). To this, dried and deaerated diethyl ether (5 mL) was added under an argon atmosphere. The resulting yellow solution was stirred for 30 min. Deaerted heptane (100 mL) was added to precipitate the complex. After stirring for 1 h, the supernatant was decanted. The remaining yellow-oily solid was dissolved again in dried and dearated diethyl ether (10 mL) and precipitated with deaerated heptane (100 mL). The resulting solid was placed in vacuo to yield 66 mg (83%) of a yellow/orange powder. Anal. Calcd: C, 53.00; H, 1.96; N, 4.94. Found: C, 52.97; H, 1.94; N, 4.95. ^{1}H NMR (CD_3NO_2): δ 8.68 (3H, s, br), 7.89 (3H, s, br), 7.44 (6H, s, br), 4.15 (6H, s).

$[Cu^I(bqpa)(CO)]B(C_6F_5)_4$ (3^{bqpa}−CO). In a 100 mL Schlenk flask equipped with a stir bar, BQPA (43 mg, 0.11 mmol) and $[Cu^I(CH_3CN)_4]B(C_6F_5)_4$ (100 mg, 0.11 mmol) were added together. To this, CO saturated Et_2O (5 mL) was added under a CO atmosphere. The resulting light-yellow solution was stirred for 30 min. CO-saturated pentane (100 mL) was added to the solution via a cannula to precipitate the product. After stirring for 1 h, a white solid precipitated. The supernatant was decanted, and the solid was placed in vacuo, yielding 106 mg (83%) of a white powder. ^{1}H NMR (CD_3NO_2): δ 8.68 (3H, s, br), 7.89 (3H, s, br), 7.44 (6H, s, br), 4.15 (6H, s).

Gas Mixing. Carbon monoxide (Air Gas East, grade 2.3) and/or a custom 1% CO-in-N_2 gas mixture (Air Gas East) were treated by passing through an R & D Separations oxygen/moisture trap (Agilent Technologies OT3−4) and mixed with nitrogen (Air Gas East, grade 4.8) through two MKS Instruments mass-flow controllers (MFCs, MKS 1179A) controlled by an MKS Instruments Multi Gas Controller (MGC, MKS 647C). The gas mixtures were determined by the set flow rates of the two gases. For example, a 10% CO mixture would be made by mixing CO at a rate of 10 standard cubic centimeters per minute (sccm) with N_2 at 90 sccm for a total flow of 100 sccm. The CO concentration in solution was determined from the percent mixture and the literature values for CO saturation (in THF $[CO]_{sat} = 0.0101$ M; in CH_3CN, $[CO]_{sat} = 0.10$ M)[47] and adjusted for solvent contraction.

UV−Vis Spectroscopy. Absorption spectra were obtained using a Hewlett-Packard 8452A or a Hewlett-Packard 8453 diode array spectrophotometer. Low temperature measurements (−80 to 0 °C) were made using a Neslab Ult-95 controller by circulating methanol through a two-window optical dewar, as previously described. High-temperature measurements (20−45 °C) were made using a Neslab Endocal circulating (1:1 ethylene glycol/water) bath. Samples were prepared in the dry box using a 10 mm quartz Schlenk cuvette (designed for low-temperature studies) equipped with a rubber serum stopper. The gas mixtures were introduced into the cuvette using a 24 in. needle and bubbling directly through the solution for ∼30 s at room temperature. Samples were equilibrated for a minimum of 3 min upon changing the temperature.

Infrared Spectroscopy. IR spectra were obtained at room temperature using a Mattson Galaxy 4030 series FTIR spectrophotometer. Samples were prepared in an inert atmosphere box. Isolated copper(I) carbonyl compounds (8−10 mg) were prepared in Nujol mull for solid-state analysis by pressing between two sodium chloride salt plates. Solutions for the infrared spectral analysis of carbonylated species were prepared by dissolving 8−10 mg in <1 mL of solvent (CH_3CN or THF) in a 1 dram vial capped with a red rubber septum. The samples were brought out of the dry box, purged with CO for ∼10 s at room temperature and reintroduced into the dry box, where the samples were transferred to a Spectralys Specac KBr plate solution-IR cell.

Cyclic Voltammetry. Studies were carried out using a Bioanalytical Systems BAS-100B electrochemistry analyzer. The air-sensitive samples were prepared in a 10 mL Schlenk flask equipped with a 14/20 rubber septum in an inert atmosphere box and comprised of a 1−3 mM solution of copper compound with 100 mM tetrabutylammonium hexafluorophosphate (supporting electrolyte) in CH_3CN. The flask was removed from the dry box, and the solution was transferred under positive argon pressure via cannula to a three-neck (25 mL) round-bottom flask equipped with a glassy-carbon working electrode, saturated calomel reference electrode, and a platinum-wire counter electrode. Each electrode was connected to the flask by piercing through a 14/20 rubber septum. An external reference of ferrocene (Fc, monitoring the Fc^+/Fc couple) under the same conditions described was also measured, $E_{1/2} = 400$ mV versus SCE.

Determination of CO Binding Constants, K_{CO} (M^{-1}). Using spectrophotometric (UV−vis) titrations of carbon monoxide and calculated extinction coefficients (M^{-1} cm^{-1}), K_{CO} could be determined using eq 1. The molar concentration of $[(L)Cu^I(CO)]^+$ was determined by eq 2 and $[(L)Cu^I]^+$ was determined by subtracting $[(L)Cu(CO)]^+$ from the total concentration of the copper compound being studied (eq 3). Plots of [CO] versus $[(L)Cu(CO)]^+/[(L)Cu]^+$ were found to be linear, and the slope affords the representative equilibrium constant. Vant Hoff analysis, eq 4, of equilibrium constants measured as a function of temperature was used to obtain thermodynamic parameters.

$$K_{CO} = \frac{k_{CO}}{k_{-CO}} = \frac{[(L)Cu^I(CO)]^+}{[(L)Cu^I]^+[CO]} \quad (1)$$

$$[(L)Cu^I(CO)]^+ = \frac{Abs_{\lambda max} - \epsilon \times [(L)Cu^I]_{TOT}}{\epsilon_{[(L)Cu(CO)]+} - \epsilon_{[(L)Cu]+}} \quad (2)$$

$$[(L)Cu^I]^+ = [(L)Cu^I]^+_{TOT} - [(L)Cu^I(CO)]^+ \quad (3)$$

$$\ln(K_{CO}) = -\frac{\Delta H^\circ}{RT} + \frac{\Delta S^\circ}{R} \quad (4)$$

Laser Flash Photolysis: Determination of the Bimolecular Rate Constant, k_{CO} (M^{-1} s^{-1}). Transient absorbance measurements were performed using a Nd:YAG (Continuum Surelite III) laser

(47) Cargill, R. W.; Battino, R. *Carbon Monoxide*, lst ed.; Pergamon Press: New York, 1990.

Table 1. Numerical Crystal and Refinement Data for the X-ray Crystal Structures

complex	$[Cu^{I}(H-tmpa)(CO)]B(C_6F_5)_4$ (**1^{H}−CO**)	$[Cu^{I}(Me_2N-tmpa)(CO)]B(C_6F_5)_4$ (**1^{Me2N}−CO**)	$[Cu^{I}(bqpa)(CO)]B(C_6F_5)_4$ (**3^{bqpa}−CO**)
formula (sum)	$C_{43}\,H_{18}\,B\,Cu\,F_{20}\,N_4\,O$	$C_{53}\,H_{43}\,B\,Cu\,F_{20}\,N_7\,O_2$	$C_{51}\,H_{22}\,B\,Cu\,F_{20}\,N_4\,O$
fw	1060.96	1264.29	1161.08
cryst syst	monoclinic	triclinic	monoclinic
space group	$P2_1/c$	$P\bar{1}$	$P2/c$
a (Å)	15.0630(9)	11.0733(10)	21.9205(7)
b (Å)	18.9983(9)	15.0029(11)	7.8885(3)
c (Å)	14.8122(11)	16.9685(16)	26.6533(10)
α (deg)	90	69.838(8)	90
β (deg)	107.037(6)	87.098(8)	96.523(3)
γ (deg)	90	84.613(7)	90
V (Å^3)	4052.8(4)	2634.1(4)	4579.0(3)
Z	4	2	4
μ/mm^{-1} (Mo Kα)	0.67587	0.52931	0.607
reflns collected (total)	36 957	35 413	49 165
R_{int} (no. of equiv. reflections)	13 927	17 308	8356
observed reflns [I/s(I) > 2]	7935	9920	6130
Final R, Rw [$I/\sigma(I)>2$]	0.0418, 0.0986	0.0609, 0.1911	0.0393, 0.0930

on a previously described apparatus.[48] Samples of copper complexes were prepared within the dry box in a 10 mm quartz cuvette equipped with a Schlenk stopcock and 14/20 joint. The samples were irradiated with 355 nm pulsed light (8−10 mJ/cm^2) and protected from the probe beam with appropriate UV filters. Kinetic data at monitored wavelengths were averages of 40 to 90 laser pulses. The CO concentrations were varied as described above (UV−vis spectroscopy) to determine the second-order rate constant, k_{CO}, using eq 5. Variable low-temperature studies (−80 to 0 °C) were performed using the setup described in previous work.[38] From the variable temperature work, Eyring analyses, eq 6, were performed to obtain activation parameters.

$$k_{obs} = k_{CO}[CO] \tag{5}$$

$$\ln\left(\frac{k_{CO} \times h}{k_B \times T}\right) = -\frac{\Delta H^{\ddagger}}{RT} + \frac{\Delta S^{\ddagger}}{R} \tag{6}$$

Comparative Actinometry. To determine quantum efficiencies, samples of the various copper complexes were prepared in a 10 mm quartz cuvette on a millimolar scale using dried and distilled THF in a dry box at room temperature. Upon removal from the dry box, the samples were sparged with CO gas. The absorbance at the excitation wavelength 355 nm was measured (for example 0.1 au) using an HP 8453 UV−vis diode array. An actinometer ($\phi_{eff} = 1$) using $[Ru(bpy)_3]Cl_2$ in THF (with the aid of excess NaBArF in situ metathesis) was prepared.[49] The actinometer solution was prepared to ensure that the measured absorbance at 355 nm matched that of the copper−carbonyl solution (for example 0.1 au). The samples were then irradiated at 355 nm, and a change in absorbance (ΔA) was measured at the corresponding λ_{max} values where the change in extinction coefficients ($\Delta\epsilon$) is known. From these data, the concentration of transient species can be measured using Beer's law ($\Delta A/\Delta\epsilon = \Delta$Concentration). Because the quantum yield for the formation of the $[Ru(bpy)_3]^{2+}$ MLCT excited state is known to be 1.00, the concentration of the excited state formed is equal to the concentration of absorbed photons. With a separate measurement of the concentration of the copper−solvento compound (CO dissociated) measured under the same conditions, the quantum yield is determined by the ratio, that is, $\phi = [(L)Cu^{I}]^{+}$/[photons].

X-ray Crystallographic Studies of (1^{H}−CO), (1^{Me2N}−CO), and (3^{bqpa}−CO). All of the crystals reported here were prepared in a dry box via the dissolution of 5 mg of copper complex in dry nitrogen-saturated diethyl ether (∼0.5 mL). The yellow solutions were transferred to a 9" NMR tube and capped with a rubber septum. The samples were removed from the drybox, and CO was sparged directly through the solution with a needle, followed by the layering of CO-saturated pentane (>98%). Colorless to light-yellow crystals were afforded after 24 h.

Crystals of each compound were placed in the N_2 cold stream at 110 K of an O.D. Xcaliber3 system equipped with a graphite monochromator and an Enhance (Mo) X-ray Source ($\lambda = 0.71073$ Å) operated at 2 kW power (50 kV, 40 mA). The detector was placed at a distance of 50 mm from the crystal. The frames were integrated with the Oxford Diffraction *CrysAlisRED* software package. All of the structures were solved and refined using the Bruker *SHELXTL* (ver. 6.1) software package. Analysis of the data showed no negligible decay. Relevant crystallographic information is given in Table 1.

Results and Discussion

Synthesis of Cu(I) Carbonyl Complexes. All of the ligands used for the present study (Chart 1) were previously synthesized and characterized (Experimental Section),[42−44,50] as were the copper(I) complexes of the substituted TMPA (R−TMPA) ligands,[42] **1^{R}** (R = Me_2N, MeO, H). Copper(I) complexes as $B(C_6F_5)_4^-$ salts with PMAP, PMEA, and BQPA are described here. Copper carbonyl complexes $[(L)Cu^{I}(CO)]B(C_6F_5)_4$, with the exception of $[Cu^{I}$(MeO-TMPA)-$(CO)]B(C_6F_5)_4$ **1^{MeO}−CO**, were isolated by 1:1 mixing of ligand and $[Cu^{I}(CH_3CN)_4]B(C_6F_5)_4$[46] in CO-saturated diethyl ether and precipitated by addition of a > 10 fold excess (by volume) of CO saturated heptane; **1^{MeO}−CO** was produced in situ by sparging LCu^{I} complex solutions with CO. The $B(C_6F_5)_4^-$ counteranion was chosen to afford greater solubility of the resulting copper complex in a wide array of solvents, in particular THF. Crystals suitable for X-ray diffraction were prepared via the slow diffusion of pentane with diethyl ether solutions of complexes under an atmosphere of CO.

(48) Bignozzi, C. A.; Argazzi, R.; Chiorboli, C.; Scandola, F.; Dyer, R. B.; Schoonover, J. R.; Meyer, T. J. *Inorg. Chem.* **1994**, *33*, 1652−1659.

(49) Yoshimura, A.; Hoffman, M. Z.; Sun, H. *J. Photochem. Photobiol. A* **1993**, *70*, 29−33.

(50) Karlin, K. D.; Shi, J.; Hayes, J. C.; McKown, J. W.; Hutchinson, J. P.; Zubieta, J. *Inorg. Chim. Acta* **1984**, *91*, L3−L7.

Scheme 2

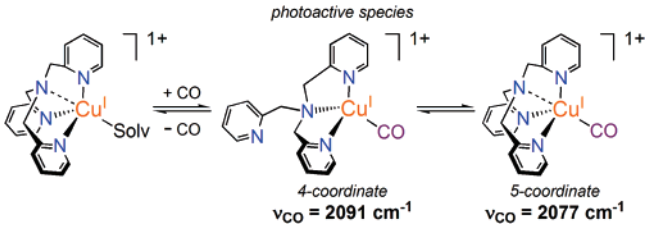

Solution and Solid-State Coordination Geometries. There is compelling evidence from the present and previous work[45,51] that one pyridyl ring of the H-TMPA ligands in $[Cu^{I}(H\text{-tmpa})(CO)]^{+}$ (**1^{H}−CO**) dissociates in solution to accommodate an ancillary ligand such as CO. In fluid solution, an equilibrium like that shown in Scheme 2 is found to exist under many experimental conditions. In fact, inductive and steric effects can be used to tune the equilibrium. This is particularly relevant to the present work, as the nominally four-coordinate species, that is, with copper(I)−ligand tridentate chelation plus the CO donor, is identified as *the* species that readily photoreleases CO (see discussion below).

X-ray Crystallography. Figure 1 shows ORTEP diagrams of $[Cu^{I}(H\text{-tmpa})(CO)]^{+}$ (**1^{H}−CO**) and $[Cu^{I}(Me_2N\text{-tmpa})(CO)]^{+}$ (**1^{Me2N}−CO**). Partial bond length and angle data are provided in the figure legend, with full details given in the Supporting Information.[52] The structures of **1^{H}−CO** and **1^{Me2N}−CO** display an overall five-coordinate geometry, which has been observed previously for related analogues such as $[Cu^{I}(H\text{-tmpa})(CH_3CN)]^{+}$ (**1^{H}**) ($Cu-N_{pyridyl(ave)}$ = 2.090(11), $Cu-N_{alkylamine}$ = 2.431(10) Å; the cuprous ion lies 0.55 Å out of the N_{py} plane toward the acetonitrile ligand).[53] Thus, the structures are more like pseudo-tetrahedral, with the three $N_{pyridyl}$ ligands ($Cu-N_{pyridyl(ave)}$ = 2.115 (15) Å) and the carbon from the CO bound as strong donors; the fifth, weakly interacting apical alkylamino nitrogen is forced out of the N_{py} plane and has a bond distance of ∼2.5 Å. For both structures (**1^{H}−CO** and **1^{Me2N}−CO**), the average $N_{pyridyl}-Cu-C$ angle is 107° and the average $N_{pyridyl}-Cu-N_{pyridyl}$ angle is 112°. Constraints induced by the ligand environment lead to a preferred four-coordinate carbonyl species (like that given in Scheme 2) when in solution (also, see IR discussion below), as well as to the established dynamic behavior of such cuprous species utilizing tetradentate chelators.[42,54] A number of overall four-coordinate copper(I)−CO complexes have been structurally characterized, and they exhibit N−Cu−C bond angles of ∼120° and N−Cu−N ∼ 95°.[55−61]

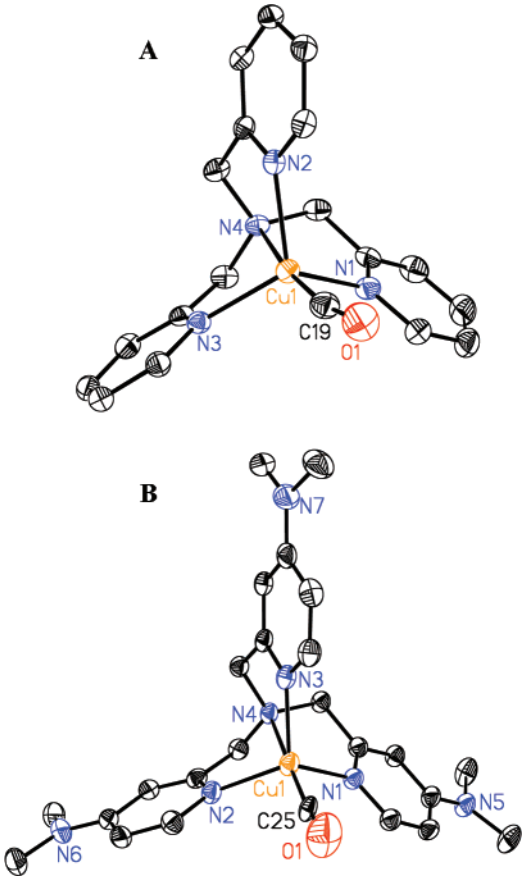

Figure 1. ORTEP diagrams of **A**. $[Cu^{I}(H\text{-tmpa})(CO)]^{+}$ (**1^{H}−CO**) and **B**. $[Cu^{I}(Me_2N\text{-tmpa})(CO)]^{+}$ (**1^{Me2N}−CO**). Hydrogen atoms and counteranions are omitted for clarity. Selected bond lengths are: **A**. Cu−C 1.852(2), C−O 1.124(2), $Cu-N_{am}$ 2.479(15), and $Cu-N_{py(ave)}$ 2.115(15) Å; and **B**. Cu−C 1.870(2), C−O 1.091(3), $Cu-N_{am}$ 2.446(2), and $Cu-N_{py}$ 2.114(8) Å.

A representation of the crystal structure of $[Cu^{I}(bqpa)(CO)]^{+}$ (**3^{bqpa}−CO**) is given in Figure 2, along with a listing of selected bond lengths. The most interesting feature of this complex is the displaced dangling quinolyl arm of the ligand (which in fact is disordered over two positions, see Supporting Information).[52] This results in a tridentate (N_3) ligand coordination mode in spite of the ligand's tetradentate (N_4) nature. The $N_{pyridyl,quinolyl}-Cu-N_{alkylamino}$ angles are quite severe (∼80°). Thus, like other tridentate ligand copper carbonyl complexes, the observed metal coordination geometry is distorted tetrahedral.[55−61]

In previous work, the crystal structure of $[Cu^{I}(bqpa)]B(C_6F_5)_4$ (**3^{bqpa}**) was obtained in which the pyridyl and both quinolyl N-donors are coordinated to the cuprous ion.[62] Note that, in the absence of CO, **3^{bqpa}** is a four-coordinate species

(51) Kretzer, R. M.; Ghiladi, R. A.; Lebeau, E. L.; Liang, H.-C.; Karlin, K. D. *Inorg. Chem.* **2003**, *42*, 3016−3025.
(52) See Supporting Information.
(53) Lim, B. S.; Holm, R. H. *Inorg. Chem.* **1998**, *37*, 4898−4908.
(54) Jacobson, R. R. Ph.D. Dissertation, State University of New York at Albany, 1989.
(55) Pasquali, M.; Marini, G.; Floriani, C.; Gaetanimanfredotti, A.; Guastini, C. *Inorg. Chem.* **1980**, *19*, 2525−2531.
(56) Kitajima, N.; Fujisawa, K.; Fujimoto, C.; Moro-oka, Y.; Hashimoto, S.; Kitagawa, T.; Toriumi, K.; Tasumi, K.; Nakamura, A. *J. Am. Chem. Soc.* **1992**, *114*, 1277−1291.
(57) Karlin, K. D.; Tyeklár, Z.; Farooq, A.; Haka, M. S.; Ghosh, P.; Cruse, R. W.; Gultneh, Y.; Hayes, J. C.; Toscano, P. J.; Zubieta, J. *Inorg. Chem.* **1992**, *31*, 1436−1451.
(58) Ardizzoia, G. A.; Beccalli, E. M.; Lamonica, G.; Masciocchi, N.; Moret, M. *Inorg. Chem.* **1992**, *31*, 2706−2711.
(59) Imai, S.; Fujisawa, K.; Kobayashi, T.; Shirasawa, N.; Fujii, H.; Yoshimura, T.; Kitajima, N.; Moro-oka, Y. *Inorg. Chem.* **1998**, *37*, 3066−3070.
(60) Conry, R. R.; Ji, G. Z.; Tipton, A. A. *Inorg. Chem.* **1999**, *38*, 906−913.
(61) Reger, D. L.; Collins, J. E. *Organometallics* **1996**, *15*, 2029−2032.
(62) Lucchese, B. Recognizing and Predicting General Trends in the Reactivity and Chemistry of a Series of Related Copper Complexes. Ph.D. Dissertation, Johns Hopkins University, 2003.

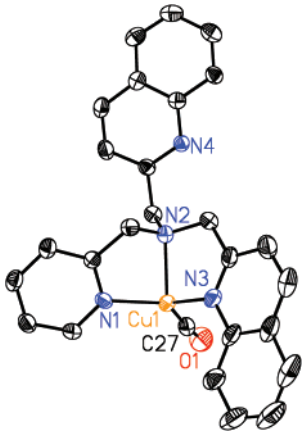

Figure 2. ORTEP diagram of $[Cu^{I}(bqpa)(CO)]^{+}$ (**3**^{bqpa}**−CO**). Hydrogen atoms and counteranions are omitted for clarity. Selected bond lengths: Cu−C 1.793(3), C−O 1.132(4), Cu−N_{am} 2.140(2), and Cu−N_{py} 2.036(2) Å.

and does not bind a solvent molecule (i.e., CH_3CN); similarly, **1**^{Me2N}, **2**^{pmea}, and **2**^{pmap} have related static structures.[42−44,62] Upon the addition of PPh_3 to **3**^{bqpa}, a quinolyl arm dissociates, resulting in a pseudo-tetrahedral complex;[44] a similar structure with a dangling pyridyl arm was observed in $[Cu^{I}(H\text{-tmpa})(PPh_3)]^{+}$.[45] Thus, the CO adduct here exhibits a similar structure. We suggest that the quinolyl arm is preferentially displaced by CO because of its greater steric bulk and demands compared to a pyridyl ligand arm. The observation of a dangling quinolyl arm in the solid-state structure of **3**^{bpqa}**−CO** plays a key role in deciphering infrared spectroscopic data (vide infra).

Infrared Spectroscopy. Evidence for equilibria like that shown in Scheme 2 was abstracted from solution (THF and CH_3CN) and solid state (Nujol mull) IR data obtained from the series of copper carbonyl compounds of **1**−**3** (Table 2). Carbon monoxide vibrational frequencies for synthetic (L)-Cu^{I}(CO) complexes[55−61,63−70] and copper carbonmonoxy proteins[7−9,16−22] fall in the range ν_{CO} = 2040−2125 cm^{-1}; in fact, protein Cu^{I}−CO adducts typically exhibit ν_{CO} values 20−40 cm^{-1} lower than model species.[69]

As described above, $[Cu^{I}(Me_2N\text{-tmpa})(CO)]^{+}$ (**1**^{Me2N}**−CO**) and $[Cu^{I}(H\text{-tmpa})(CO)]^{+}$ (**1**^{H}**−CO**) exhibit solid-state tetrahedral-like structures with all of the pyridyl nitrogens coordinated. Corresponding Nujol mull IR spectra reveal single ν_{CO} values of 2055 and 2077 cm^{-1}, respectively. A clear substituent effect is observed with the more-electron-releasing Me_2N−TMPA ligand, substantially lowering ν_{CO} because of increased π back-bonding. However, when these complexes are dissolved in CH_3CN, the ν_{CO} values shift significantly to higher energy, by 15−19 cm^{-1}, Table 2. The loss of a pyridyl nitrogen donor is entirely consistent with weaker π back-bonding resulting in a stronger CO bond and thus a higher ν_{CO} value. By contrast, in THF solvent, two IR bands are observed for **1**^{Me2N}**−CO**, which reasonably correspond to the ν_{CO} values for the individual pure isomers (four-coordinate and five-coordinate), thus an equilibrium mixture exists (Scheme 2). In fact, the Cu(I)−carbonyl complex of MeO−TMPA displays similar behavior, except that a mixture also exists in the solid state; two ν_{CO} values are observed in the IR spectra,[52] corresponding to each isomer form (Table 2).

Additional evidence for the conclusion presented here come from a previous study where we investigated the IR spectrum of $[Cu^{I}(PY1)(CO)]^{+}$ {PY1 = the tridentate ligand bis-(2-picolyl)amine; Chart 2}.[51] Notably, ν_{CO} = 2092 cm^{-1} in CH_3CN for this complex exactly corresponds to that found for **1**^{H}**−CO** (Table 2). Thus, in solution the R−TMPA copper carbonyl complexes **1**^{R}**−CO** possess displaced pyridyl arms, and the cuprous ion is in an N_3 coordination environment that does not resemble their respective crystal structures.

Unlike the R−TMPA complexes **1**^{R}**−CO**, solution (THF and CH_3CN) and solid-state IR spectra for **3**^{bqpa}**−CO** indicate very similar ν_{CO} values (2091−2095 cm^{-1}, Table 2); thus solution and solid-state structures must be like that observed in the X-ray structure (vide supra) of **3**^{bqpa}**−CO**, with BQPA behaving as a tridentate ligand possessing a dangling quinolyl arm.

With ligands where additional methylene groups were placed between the tertiary alkylamine and the pyridyl arms, as in complex **2**^{pmea}**-CO** and **2**^{pmap}**-CO** (Chart 1), a single carbonyl stretching frequency (ν_{CO} = 2091_{ave} cm^{-1}) is observed in both CH_3CN and THF solvents (Table 2). This is consistent with N_3 ligand binding in solution. Note that solid-state carbonyl complexes could not be isolated because of the relatively low affinity of the cuprous compound precursors **2**^{R} for CO, corroborated by K_{CO} measurements (vide infra). In fact, in $[Cu^{I}(tepa)]^{+}$ (tepa = tris(2-pyridylethyl)amine), with all of ligand arms expanded to $-CH_2CH_2-$ moieties, there was no evidence for CO coordination to copper in solution or in the solid state.

In summary, carbon monoxide acts as a very good ligand for these tripodal tetradentate ligand−copper(I) complexes and leads to a number of structural possibilities, overall five-coordinate and/or four-coordinate (with dangling ligand arm) structures, as deduced by a combination of X-ray diffraction studies and IR spectroscopy. This ability to distinguish between four- and five-coordinate copper systems will aid in determining the ligand environment responsible for CO photodissociation (vide infra).

Electrochemical Studies. Cyclic voltammetric measurements were carried out on 100 mM CH_3CN solutions of copper(I) complexes **1**−**3** (Chart 1). The copper(II/I) redox chemistry is classified as quasi-reversible because the anodic and cathodic currents were approximately equal and the peak-

(63) Sorrell, T. N.; Jameson, D. L. *J. Am. Chem. Soc.* **1983**, *105*, 6013−6018.
(64) Sorrell, T. N.; Malachowski, M. R. *Inorg. Chem.* **1983**, *22*, 1883−1887.
(65) Gagne, R. R.; Allison, J. L.; Gall, R. S.; Koval, C. A. *J. Am. Chem. Soc.* **1977**, *99*, 7170−7178.
(66) Gagne, R. R.; Koval, C. A.; Smith, T. J.; Cimolino, M. C. *J. Am. Chem. Soc.* **1979**, *101*, 4571−4580.
(67) Nelson, S. M.; Lavery, A.; Drew, M. G. B. *J. Chem. Soc., Dalton Trans.* **1986**, 911−920.
(68) Schindler, S.; Szalda, D. J.; Creutz, C. *Inorg. Chem.* **1992**, *31*, 2255−2264.
(69) Rondelez, Y.; Séneque, O.; Rager, M.-N.; Duprat, A. F.; Reinaud, O. *Chem.−Eur. J.* **2000**, *6*, 4218−4226.
(70) Hernandez, R. M.; Aiken, L.; Baker, P. K.; Kalaji, M. *J. Electroanal. Chem.* **2002**, *520*, 53−63.

Table 2. Carbonyl Stretching Frequencies for $[(L)Cu^{I}(CO)]^{+}$ Complexes and Cyclic Voltammetry Data for Cu(I) Complexes

compound	Nujol mull (cm^{-1})	CH_3CN (cm^{-1})	THF (cm^{-1})	$E_{1/2}$ [c] (mV vs Fc^{+}/Fc)
$[Cu^{I}(Me_2N-tmpa)(CO)]^{+}$ (**1^{Me2N}−CO**)	2055	2074[a]	2049,2077	−700
$[Cu^{I}(MeO-tmpa)(CO)]^{+}$ (**1^{MeO}−CO**)	2067,2091	2087[a]	2063,2085	−490
$[Cu^{I}(H-tmpa)(CO)]^{+}$ (**1^{H}−CO**)	2077	2092[a]	2090	−400
$[Cu^{I}(pmea)(CO)]^{+}$ (**2^{pmea}−CO**)	[b]	2093	2091	−360
$[Cu^{I}(pmap)(CO)]^{+}$ (**2^{pmap}−CO**)	[b]	2090	2089	−250
$[Cu^{I}(bqpa)(CO)]^{+}$ (**3^{bqpa}−CO**)	2095	2093	2091	−210

[a] Previously measured.[42] [b] Solid-state samples could not be isolated. [c] Measurements on copper(I) complexes **1**−**3** (not carbonyl) in CH_3CN under a N_2 atmosphere.

Chart 2

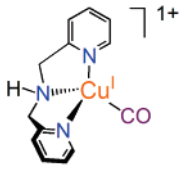

$[Cu^{I}(PY1)(CO)]^{+}$

ν_{CO} = 2092 cm^{-1}

to-peak separation was greater than 60 mV (Table 2). Comparisons to a ferrocene (Fc) and Fc/Fc^{+} internal standard redox couple showed that the voltammograms represent single electron-transfer processes. In fact and not unexpectedly, a nice correlation exists between the copper(II/I) reduction potentials ($E_{1/2}$, Table 2) and the ν_{CO} frequencies. The complexes with more-electron-donating ligand possess more-negative $E_{1/2}$ values while displaying lower-energy carbon monoxide stretches. This is straightforwardly explained, because a complex with greater $E_{1/2}$ will have a ligand with poor donating ability (favoring a lower oxidation state) and thus ν_{CO} will decrease.

In separate experiments, the carbonyl compounds **1**−**CO** through **3**−**CO** only exhibit irreversible oxidations at more-positive potentials than seen in the absence of CO (data not shown). This is in contrast to the case for many copper(I)−carbonyl species where the increasing [CO] a reversible electrochemical wave shifts to more-positive $E_{1/2}$ values; such data has been used to calculate the equilibrium CO binding constants.[65,66,68,71] Subtractively normalized interfacial FTIR spectroscopy (SNIFTIRS) experiments conducted by Hernandez and co-workers[70] indicated that the oxidation of LCu^{I}−CO to Cu(II) results in the loss of the carbonyl signal from the complex; however, the reduction of Cu(II) to Cu(I) under CO results in the reappearance of the LCu^{I}−CO complex.

Equilibrium CO Binding (K_{CO}) in CH_3CN. Carbon monoxide binds to the copper(I) complexes under study to varying degrees. In fact, there is surprisingly limited literature on the quantitative study of CO interactions with copper(I) complexes. The techniques that have been employed to measure equilibrium binding constants include spectrophotometric,[65] electrochemical,[66,68,71] and manometric[63,64,67] methods.

Spectrophotometric titrations of carbon monoxide into submillimolar concentrations of copper(I) compounds **1**−**3** were used to determine equilibrium binding constants, K_{CO} (M^{-1}) in CH_3CN and THF. The copper(I) complexes display a broad absorption band between 300 and 360 nm in both solvents, this absorption is assigned as a metal-to-ligand charge-transfer (MLCT) transition on the basis of the intensity and energy. These MLCT absorptions undergo a significant blue-shift upon the addition of CO, consistent with the positive shift of the Cu(I) → Cu(II) oxidation observed by cyclic voltammetry. Linear plots of [CO] versus $[(L)Cu^{I}(CO)]^{+}/[(L)Cu^{I}]^{+}$ afford slopes equal to K_{CO} (eq 2, Experimental Section and Figure 3). The equilibrium constants were also measured as a function of temperature from 233 to 313 K. Thermodynamic parameters (Table 3) were then abstracted from Van't Hoff analyses of the data (Experimental Section, eqs 1−4; and Supporting Information).[52]

The Me_2N− versus MeO− versus H− substituted TMPA copper(I) complexes (**1^{R}**) display significant variation in CO-binding properties attributable to the difference in electron-donating ability of the ligand 4-pyridyl substituents. Binding studies in CH_3CN reveal that $[Cu^{I}(Me_2N\text{-tmpa})(CH_3CN)]^{+}$ (**1^{Me2N}**), which has the most-negative $Cu^{II/I}$ redox potential (Table 2), coordinates CO stronger than all of the compounds investigated ($K_{CO} \approx 8000\ M^{-1}$, Table 3).[52] In fact, K_{CO} for **1^{Me2N}** is so large that a custom 1% CO-in-N_2 gas mixture was necessary to quantify thermodynamic parameters ($\Delta H° = -40.8$ kJ mol^{-1}, $\Delta S° = -64.6$ J mol^{-1} K^{-1}) within the temperature range of 283−313 K. Weaker donor ligands such as in **1^{MeO}** and **1^{H}** have significantly diminished equilibrium binding constants ($K_{CO} = 780$ and 220 M^{-1}, respectively, Table 3). For **1^{Me2N}** and **1^{MeO}**, the $\Delta H°$ values are considerably more favorable (i.e., more negative) than for **1^{H}**, accounting for the large differences in K_{CO} values. However, as revealed by the thermodynamic parameters listed in Table 3, $\Delta H°$ values do not vary systematically, with **1^{MeO}** ($\Delta H° = -48.7$ kJ mol^{-1}) being more negative than **1^{Me2N}**; the entropy changes compensate such that K_{CO} values for the series decrease monotonically, **1^{Me2N}** > **1^{MeO}** > **1^{H}**.

For $[Cu^{I}(pmea)]^{+}$ (**2^{pmea}**) and $[Cu^{I}(pmap)]^{+}$ (**2^{pmap}**), where the chelate ring size increases relative to TMPA, rather-low K_{CO} values (Table 3) were observed, 150 and 2.1 M^{-1}, respectively. The K_{CO} values nevertheless align with their observed redox potentials and ν_{CO} values (Table 2); PMAP is a better donor to the cuprous ion, having high $E_{1/2}$ and ν_{CO} values. The K_{CO} and thermodynamic parameters for **2^{pmea}**, **2^{pmap}**, and **1^{H}** are roughly in the same range. We suggest that the systematic decrease in K_{CO} on going form **1^{H}** to **2^{pmea}** to **2^{pmap}** (220 to 2.1 M^{-1}) may reflect increased steric demand for CO binding to the copper(I) center; with

(71) Nanda, K. K.; Addison, A. W.; Paterson, N.; Sinn, E.; Thompson, L. K.; Sakaguchi, U. *Inorg. Chem.* **1998**, *37*, 1028−1036.

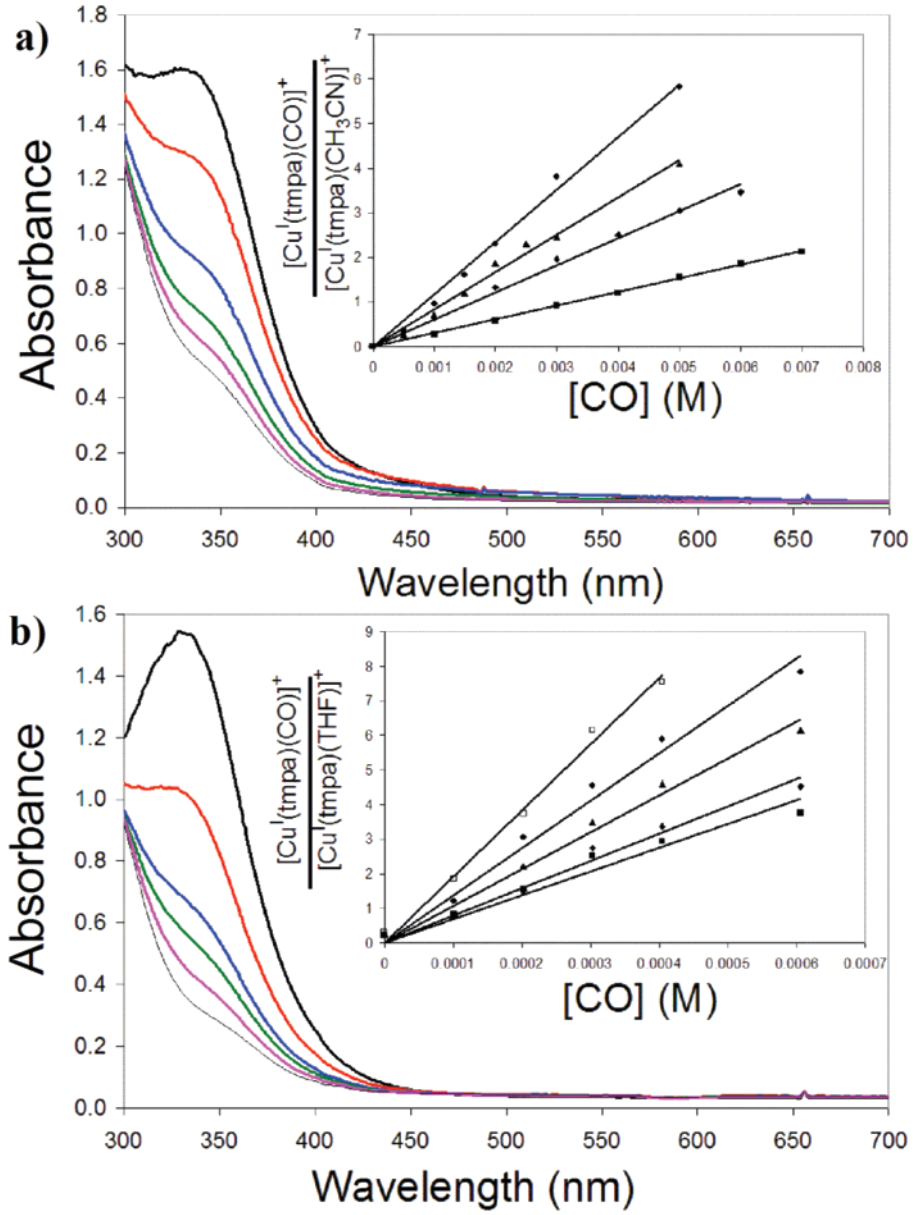

Figure 3. Spectrophotometric titration of CO to $[Cu^{I}(H\text{-tmpa})(solvent)]^{+}$ ($\mathbf{1^H}$) in **(a)** CH_3CN and **(b)** THF at room temperature. **(a)** Black, [CO] = 0.0 mM; red, [CO] = 1.0 mM; blue, [CO] = 3.0 mM; green, [CO] = 5.0 mM; magenta, [CO] = 7.0 mM; thin black, [CO] = 10 mM. The inset represents the linear plots of $[Cu^{I}(H\text{-tmpa})(CO)]^{+}/[Cu^{I}(H\text{-tmpa})(CH_3CN)]^{+}$ (i.e., [$\mathbf{1^H}$−**CO**]/[$\mathbf{1^H}$]) versus [CO] at various temperatures in CH_3CN solvent: Squares, 253 K; diamonds, 263 K; triangles, 273 K; circles, 293 K. **b)** Black, [CO] = 0.0 mM; red, [CO] = 0.1 mM; blue, [CO] = 0.2 mM; green, [CO] = 0.3 mM; magenta, [CO] = 0.4 mM; thin black, [CO] = 10 mM. The inset represents the linear plots of $[Cu^{I}(H\text{-tmpa})(CO)]^{+}/[Cu^{I}(H\text{-tmpa})(thf)]^{+}$ (i.e., [$\mathbf{1^H}$−**CO**]/[$\mathbf{1^H}$]) versus [CO] at various temperatures in THF solvent: Squares, 293 K; diamonds, 298 K; triangles, 303 K; circles, 308 K; open squares, 313 K.

longer chelate arms, the copper(I) is more fully surrounded by the tetradentate ligand framework.

Carbon monoxide binding to $[Cu^{I}(bqpa)]^{+}$ ($\mathbf{3^{bqpa}}$) was expected to be poor, because of the steric constraints of the large quinolyl moieties. On the contrary, CO binds somewhat more strongly to $\mathbf{3^{bqpa}}$, K_{CO} = 660 M^{-1}, than to $\mathbf{1^H}$, K_{CO} = 220 M^{-1} (Table 3), in CH_3CN. This observation contrasts with the relationship between redox potentials and CO binding observed for the other copper pyridylalkylamine complexes (vide supra). Van't Hoff analysis indicates a much more favorable standard enthalpy of the CO reaction with $\mathbf{3^{bqpa}}$ ($\Delta H°$ = −36.7 compared to −25.7 kJ mol^{-1} for $\mathbf{1^H}$) while accompanied by a more negative entropy change ($\Delta S°$ = −72.2 compared to −41.3 J mol^{-1} K^{-1} for $\mathbf{1^H}$) (Table 3). These differences in thermodynamic parameters suggest that solvent ligation is critical and leads to differing behavior for CO binding to $\mathbf{3^{bqpa}}$ compared to $\mathbf{1^H}$, Scheme 3. Acetonitrile does not coordinate to Cu(I) in $\mathbf{3^{bqpa}}$ (vide supra), leading to a highly negative entropy for the formation of $\mathbf{3^{bqpa}}$−CO. In contrast, the loss of a CH_3CN ligand must occur prior to CO coordination to $\mathbf{1^H}$.

Carbon Monoxide Binding in THF; Solvent Effects. Carbon monoxide binding to the copper(I) complexes under study was also examined in THF solvent, which is a very weak ligand (if at all) for cuprous ion. In fact, there is a greater than 500-fold increase in K_{CO} for $[Cu^{I}(tmpa)(Solv)]^{+}$ ($\mathbf{1^H}$) in THF versus CH_3CN. The K_{CO} values could not be obtained for the more strongly binding ligand complexes

Table 3. Kinetic and Thermodynamic Parameters for Various Copper Complexes (Constants Reported at 298 K)[a]

compound in CH_3CN	K_{CO}	$\Delta H°$	$\Delta S°$	k_{CO}	$\Delta H^{‡}$	$\Delta S^{‡}$	k_{-CO}	$\Delta H^{‡}$	$\Delta S^{‡}$
$[Cu^I(Me_2N-tmpa)(CO)]^+$ (**1^{Me2N}–CO**)	8000	−40.8	−64.6	1.6×10^8	[b]	[b]	1.79×10^4	n/a	n/a
$[Cu^I(MeO-tmpa)(CO)]^+$ (**1^{MeO}–CO**)	780	−48.7	−108	4.8×10^7	11.7	−58.6	6.28×10^4	60.7	50.6
$[Cu^I(H-tmpa)(CO)]^+$ (**1^{H}–CO**)	220	−25.7	−41.3	5.9×10^7	17.9	−36.1	2.68×10^5	43.6	5.2
$[Cu^I(pmea)(CO)]^+$ (**2^{pmea}–CO**)	150	−32.8	−68.2	[c]	[c]	[c]	[c]	[c]	[c]
$[Cu^I(pmap)(CO)]^+$ (**2^{pmap}–CO**)	2.1	−21.9	−45.4	[c]	[c]	[c]	[c]	[c]	[c]
$[Cu^I(bqpa)(CO)]^+$ (**3^{bqpa}–CO**)	660	−36.7	−72.2	4.6×10^6	12.9	−74.1	6.97×10^3	49.6	−1.9

compound in THF	K_{CO}	$\Delta H°$	$\Delta S°$	k_{CO}	$\Delta H^{‡}$	$\Delta S^{‡}$	k_{-CO}	$\Delta H^{‡}$[d]	$\Delta S^{‡}$[d]
$[Cu^I(H-tmpa)(CO)]^+$ (**1^{H}–CO**)	1.25×10^5	−35.9	−42.6	1.92×10^9	7.13	−43.3	1.54×10^4	43.0	−0.7
$[Cu^I(pmea)(CO)]^+$ (**2^{pmea}–CO**)	140	−38.1	−86.9	[c]	[c]	[c]	[c]	[c]	[c]
$[Cu^I(pmap)(CO)]^+$ (**2^{pmap}–CO**)	6.0	−28.4	−80.4	[c]	[c]	[c]	[c]	[c]	[c]
$[Cu^I(bqpa)(CO)]^+$ (**3^{bqpa}–CO**)	2730	−44.7	−84.2	3.00×10^7	5.35	−83.8	1.10×10^4	50.05	0.4

[a] Units of kinetic and thermodynamic values are as follows: K_{CO}, M^{-1}; k_{CO}, M^{-1} s^{-1}; k_{-CO}, s^{-1}; ΔH, kJ mol^{-1}; ΔS, J mol^{-1} K^{-1}. [b] Data analysis complicated by excited-state formation and the inability to confidently obtain k_{CO}. See Discussion for details. [c] No evidence for CO photodissociation was obtained. [d] See Supporting Information for Van't Hoff plots. [e] n/a = not available.

Scheme 3

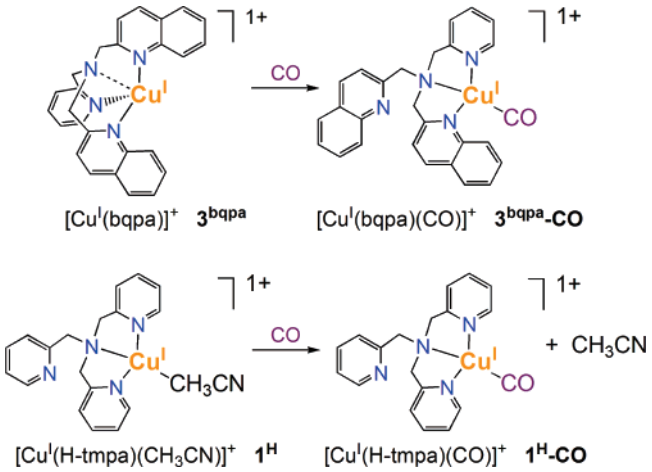

1^{MeO} and **1^{Me2N}** because the CO binding affinity was too great; the equilibrium lies too far to the right, that is toward $[(L)Cu^I(CO)]^+$. Even with the use of a 1% CO-in-N_2 gas mixture, measurable differences in concentration were not observed. The origin of the enhanced binding of CO in THF is enthalpic (Table 3).

In contrast to the behavior observed in CH_3CN, CO binds more favorably to $[Cu^I(tmpa)(thf)]^+$ (**1^{H}**) than $[Cu^I(bqpa)]^+$ (**3^{bqpa}**) in THF solvent by greater than four orders of magnitude (Table 3). The stronger CO binding in THF now follows expectations in terms of observed copper(I) complex redox potentials ($E_{1/2}$) and ν_{CO} values, that is, TMPA is inherently a better donor ligand to copper. Acetonitrile binding and the lack thereof for **3^{bqpa}** thus caused the switch in affinities. Notice that the enthalpic term for the Cu(I)−CO interaction is much more favorable when solvent binding is not a factor; in THF versus CH_3CN, $\Delta H°$ decreases by 10.2 kJ mol^{-1} for CO binding to **1^{H}** and by 8.0 kJ mol^{-1} for **3^{bqpa}**. Further examination of Table 3 shows that the reaction entropies for **1^{H}** and **3^{bqpa}** are nearly independent of the solvent.

Examination of the K_{CO} data obtained for $[Cu^I(pmea)]^+$ (**2^{pmea}**) and $[Cu^I(pmap)]^+$ (**2^{pmap}**) (Table 3) indicates that the solvent has little effect on equilibrium binding constants and thermodynamic parameters. This is consistent with the chemistry previously observed for these complexes,[43] in that there is no evidence for solvent coordination (i.e., of solvent molecules) beyond the N_4 donation by the tetradentate ligands. As previously mentioned, the extended ligand arms and resulting increased chelate ring satisfies the coordination needs of the cuprous ion.

Summary of CO-Binding Eqilibrium Data. Through spectrophotometic titrations, quantitative insights into CO binding to copper(I) coordination complexes have been obtained. As expected from basic coordination chemistry principles, the electron-donating ability of the ligand as well as the geometry have an effect on the equilibrium constants. Increasing the electron-donating ability of the ligand, such as in **1^{R}**, leads to enhanced CO-binding affinities; however, increasing the chelate ring size of the ligand, such as in **2^{R}**, leads to a lower affinity for CO. The effect of solvent (CH_3CN) ligation is significant for **1^{H}** and results in differing CO binding behavior for **3^{bqpa}**.

It is of interest to note that our equilibrium constants are consistent with those previously measured for other copper complexes. Nelson and co-workers measured CO binding to a series of copper(I) coordination complexes with acyclic Schiff-base ligands possessing three nitrogen donors, K_{CO} = 1.6−32.1 M^{-1}.[67] The bulkiness of the ligands lead to weak CO interactions and are thus similar to what we observe for **3^{bqpa}**. In a complex that is sterically unhindered, Gagné and co-workers used an N_4 macrocycle, LBF_2 (LBF_2 = 1,1-difluoro-4,5,11,12-tetramethyl-1-bora-3,6,10,13-tetraaza-2,-14-dioxacyclotetradeca-3,5,10,12-tetraenate), to examine CO binding properties.[65] The copper(I) ion in $[Cu(LBF_2)(CO)]$ rests a full 0.96 Å out of the N_4 plane, such that, when CO binds, an unusual five-coordinate copper−carbonyl complex forms. The out-of-the-plane coordination results in a large binding constant ($K_{CO} = 4.7 \times 10^4$ M^{-1}) similar to what we observe in our R−TMPA copper complexes, **1^{R}**.

Enhanced CO binding affinities have also been observed in binuclear dicopper ligand systems. Gagné et al.[66] measured the equilibrium constant for a single CO molecule binding to a mixed-valence Cu(II)−Cu(I) complex as $K_{CO} = 2.8 \times 10^4$ M^{-1}, and Schindler et al.[68] measured the binding of two CO molecules per binuclear copper(I) complex as 1.4×10^4 M^{-1} per Cu(I). The latter binucleating ligand system {1,3-bis[bis(2-pyridylmethyl)amino]benzene} contains the same

six-membered chelate moiety, as found in $\mathbf{2^R}$. The higher binding affinity in Schindler's system is most likely due to the absence of a third pyridyl donor per copper, making for a more coordinatively unsaturated complex. In a rigid binuclear copper(I) system, Nanda et al. concluded that ligand flexibility has a more effective influence on CO-adduct formation than increased donor basicity.[71]

Sorrell and co-workers investigated CO binding to coordinatively unsaturated copper(I) complexes containing two- and three-coordinate ligands, resulting in extremely low binding affinities.[63,64] Among the series of two-coordinate copper(I) species with unidentate N-donor ligands, CuL_2^+, the bis(imidazole) analogues do not readily react with CO.[63] The natural assumption is that this is due to steric constraints from complexation with additional imidazolyl nitrogen-donors forming CuL_4^+; however, the addition of excess ligand such as 4-methylimidazole (4-MeIm) to $[Cu(4\text{-}MeIm)_2]^+$ promotes CO coordination. Therefore, the inertness of the linear two-coordinate copper(I) complexes is due to their electronic structure and greater orbital mixing, leading to shorter Cu−N bonds (∼1.87 Å). In a separate study, the low equilibrium constants for tridentate pyrazolyl copper(I) complexes binding CO are attributed to greater stability of the decarbonylated form.[64] Similar to the two-coordinate Cu(I) species, stabilization requires greater overlap between the bonding orbitals on copper and those of the ligand pyrazole nitrogens.

CO Photodissociation and Thermal Coordination Kinetics in CH_3CN (k_{CO}). As indicated in the introductory material, a new aspect of the present work is to accompany equilibrium measurements with kinetic parameters in Cu(I)−CO reactions. Kinetic analysis of CO coordination to copper was accomplished through laser flash photolysis experiments carried out between 193 and 318 K. Nanosecond absorption spectroscopic evidence shows that CO photodissociation occurs upon single-wavelength 355 nm excitation of the copper carbonyl compounds $[Cu^I(Me_2N\text{-tmpa})(CO)]^+$ ($\mathbf{1^{Me2N}-CO}$), $[Cu^I(MeO\text{-tmpa})(CO)]^+$ ($\mathbf{1^{MeO}-CO}$), $[Cu^I(tmpa)(CO)]^+$ ($\mathbf{1^H-CO}$),[36] and $[Cu^I(bqpa)(CO)]^+$ ($\mathbf{3^{bqpa}-CO}$). Following photoinitiated loss of CO, these compounds change from nearly colorless solutions to weakly yellow, as indicated by the positive absorption changes with maxima in the range of 320−360 nm that tail into the visible region. The differences in extinction coefficients ($\Delta\epsilon$) range from 3000 to 7000 M^{-1} cm^{-1}. Subsequent to photodissociation, CO rebinds to the cuprous ion, making for a fully reversible process (Scheme 1). Simulated absorption difference spectra calculated from the solvento (or naked) species minus the carbonyl species are in excellent agreement with the observed transient data, that is, $Abs[Cu^I(tmpa)(solvent)]^+ - Abs[Cu^I(tmpa)(CO)]^+$. Thus, for these copper−carbonyl complexes, photolysis results in CO dissociation and formation of the otherwise isolable solvated or unsolvated $[(L)Cu^I]^+$ complexes, followed by CO rebinding. Representative data observed after pulsed laser excitation of $\mathbf{1^H-CO}$ is shown in Figure 4; corresponding information for the other complexes is given in the Supporting Information.[52]

Such behavior has never before been observed for copper complexes ($\mathbf{1^H-CO}$ was the first reported example).[36] Previous studies photolyzing copper(I) carbonyl complexes[72,73] and/or carbonmonoxy copper proteins[74−76] resulted in luminescence and no observed CO dissociation from the metal center.

For the R−TMPA copper complexes $\mathbf{1^R}$, it was expected that the electron-donating ability of the ligand would influence the CO-binding rate constant (k_{CO}) as follows: $\mathbf{1^{Me2N}-CO} > \mathbf{1^{MeO}-CO} > \mathbf{1^H-CO}$. Complying with this trend, CO binding to $\mathbf{1^{Me2N}}$ in CH_3CN indeed possesses the greatest rate constant (k_{CO} (298 K) = 1.6×10^8 M^{-1} s^{-1}, Table 3). Activation parameters for $\mathbf{1^{Me2N}}$ were not obtained because of competing photophysical events observed at lower temperatures; details of such aspects will be the subject of a future publication. The rate constants for CO rebinding to $\mathbf{1^{MeO}}$ and $\mathbf{1^H}$ in CH_3CN are similar with k_{CO} (298 K) = 4.8×10^7 and 5.9×10^7 M^{-1} s^{-1}, respectively. It was hypothesized that the rate constant for $\mathbf{1^{MeO}}$ would be larger than that for $\mathbf{1^H}$ because of the more-electron-rich copper center. The unexpected trend is attributed to CH_3CN binding more favorably to $\mathbf{1^{MeO}}$ than $\mathbf{1^H}$, which competitively decreases the rate at which CO binds to copper. Eyring analysis indicates a favorable/lower enthalpy of activation for $\mathbf{1^{MeO}}$, but the overall rate constant was compromised by the more-negative activation entropy (Table 3). This reaction entropy value may comment on the extent to which the pyridyl arm of the ligand is coordinated (N_4) versus uncoordinated (N_3) in the transition state (Scheme 4). However, these values are relative to the coordination environment (N_3 vs N_4) of the starting complexes, making it difficult to compare the parameters of one system to another.

The rate of CO recombination to $[Cu^I(bqpa)]^+$ ($\mathbf{3^{bqpa}}$) in CH_3CN is k_{CO} (298 K) = 4.6×10^6 M^{-1} s^{-1}. The activation parameters ($\Delta H^{\ddagger}$, 12.9 kJ mol^{-1}; $\Delta S^{\ddagger}$, −74.1 J mol^{-1} K^{-1}) are both lower than those obtained for CO binding to $\mathbf{1^H}$, resulting in a smaller rate constant. We suggest that the bulky quinolyl arms of the BQPA ligand sterically hinder CH_3CN from strongly coordinating to $\mathbf{3^{bqpa}}$ (as stated previously), therefore the lower activation energy for CO rebinding to $\mathbf{3^{bqpa}}$ in comparison to $\mathbf{1^H}$ is due to diminished CO/CH_3CN competition.

Effects of Solvent Upon CO Recombination (k_{CO}). In THF solvent, CO photodissociation was spectroscopically observable, and analyses could be carried out for $\mathbf{1^H-CO}$ and $\mathbf{3^{bqpa}-CO}$. The quantum yields (ϕ) for CO photodissociation were determined by comparative actinometry: $\mathbf{1^H-CO}$, $\phi = 1.00 \pm 0.02$ and $\mathbf{3^{bqpa}-CO}$, $\phi = 0.30 \pm 0.02$. Under the same conditions in THF, photoexcitation of $\mathbf{1^{Me2N}-CO}$ and $\mathbf{1^{MeO}-CO}$ exhibits absorption features in the visible region, suggestive of a MLCT excited-state, in addition to the expected CO rebinding; as stated previously, this will

(72) Sorrell, T. N.; Borovik, A. S. *Inorg. Chem.* **1987**, *26*, 1957−1964.
(73) Sorrell, T. N.; Borovik, A. S. *J. Am. Chem. Soc.* **1987**, *109*, 4255−4260.
(74) Kuiper, H. A.; Agro, A. F.; Antonini, E.; Brunori, M. *Proc. Natl. Acad. Sci-Biol* **1980**, *77*, 2387−2389.
(75) Finazziagro, A.; Zolla, L.; Flamigni, L.; Kuiper, H. A.; Brunori, M. *Biochemistry* **1982**, *21*, 415−418.

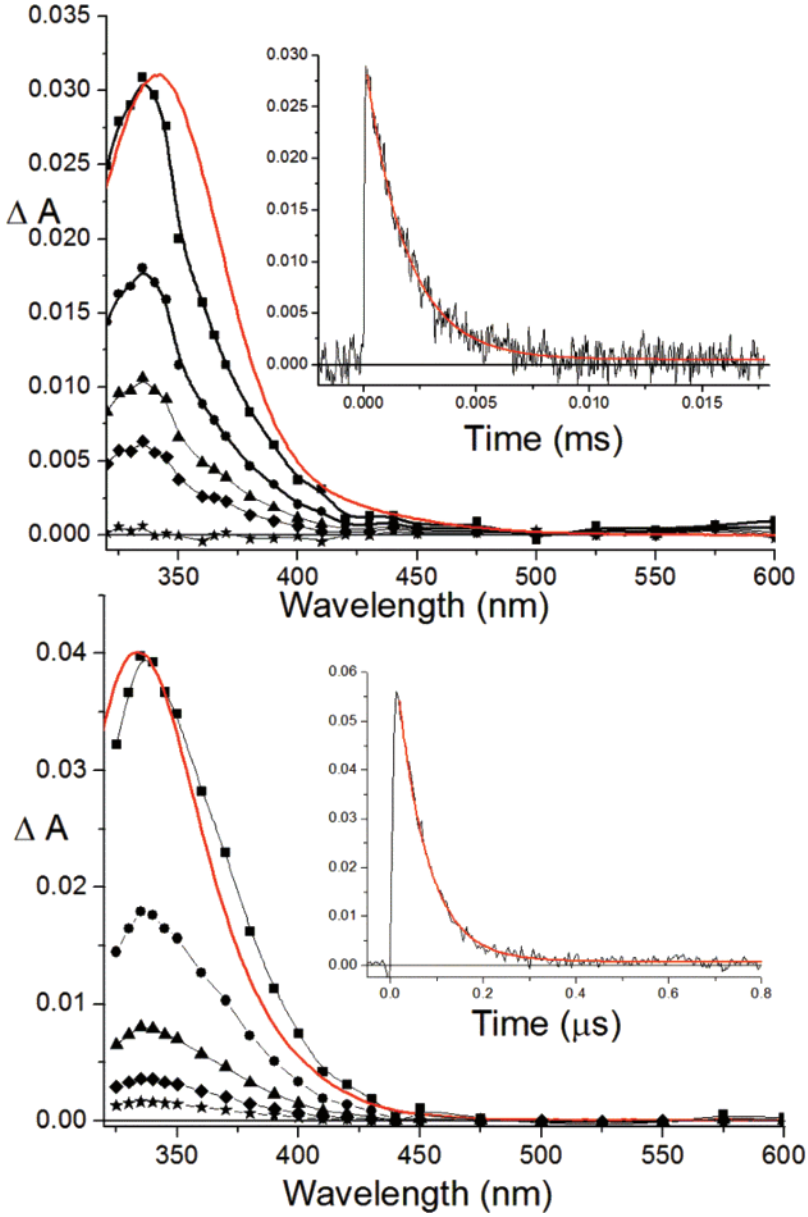

Figure 4. Transient absorption difference spectra observed after 355 nm light excitation of $[Cu^{I}(H\text{-tmpa})(CO)]^{+}$ (**1^{H}−CO**) in CH_3CN (top) and THF (bottom) at room-temperature that result in CO dissociation and the formation of $[Cu^{I}(H\text{-tmpa})(solvent)]^{+}$ (**1^{H}**) and subsequent observable recombination shown at various delay times. In CH_3CN (top) squares, 0 μs; circles, 1 μs; triangles, 2 μs; diamonds, 3 μs; and stars, 10 μs. A calculated difference spectrum of $[Cu^{I}(H\text{-tmpa})(CH_3CN)]^{+} - [Cu^{I}(H\text{-tmpa})(CO)]^{+}$ in CH_3CN is shown in red. A kinetic trace (top inset) following CO recombination to copper at 350 nm with a first-order fit, $k_{obs} = 5.5 \times 10^{5}$ s^{-1}, shown in red. In THF (bottom) squares, 0 ns; circles, 50 ns; triangles, 100 ns; diamonds, 150 ns; and stars, 200 ns. A calculated difference spectrum of $[Cu^{I}(H\text{-tmpa})(THF)]^{+} - [Cu^{I}(H\text{-tmpa})(CO)]^{+}$ in THF is shown in red. A kinetic trace (bottom inset) following CO recombination to copper at 330 nm with a first-order fit, $k_{obs} = 1.6 \times 10^{6}$ s^{-1}, shown in red.

be discussed elsewhere. Spectroscopic evidence for CO photodissociation was not observed for $[Cu^{I}(pmea)(CO)]^{+}$ (**2^{pmea}−CO**) nor $[Cu^{I}(pmap)(CO)]^{+}$ (**2^{pmap}−CO**) in either solvent.

Acetonitrile acts as a much better ligand to Cu(I) than THF. Therefore, CO rebinds to copper faster in the weakly coordinating noncompeting solvent THF. When changing from CH_3CN to THF, the rate constant (k_{CO} at 298 K) for **1^{H}** increased by greater than 3 orders of magnitude, whereas that for **3^{bqpa}** increased by slightly less than 1 order of magnitude (Table 3).[52] The coordination of CH_3CN is strongly implied in the enthalpy of the activation term for **1^{H}** and **3^{bqpa}**. When changing from CH_3CN to THF in **1^{H}**, $\Delta H^{\ddagger}$ significantly decreases by 10.8 kJ/mol. In the more sterically hindered case, **3^{bqpa}**, the trend continues with $\Delta H^{\ddagger}$ decreasing by 7.6 kJ/mol. Upon changing from coordinating to non-coordinating solvent, the decreased enthalpic barrier indicates that the de-ligation of CH_3CN precedes CO rebinding. The solvent change has very small affects on the $\Delta S^{\ddagger}$ terms, suggesting that the greatest contributor to the overall rate of recombination is the bond-formation process.

The nearly solvent-independent activation entropies ($\Delta S^{\ddagger}$) are very close in value to the actual overall reaction entropies ($\Delta S°$) (Table 3). This similarity indicates a transition state

(76) Beltramini, M.; Dimuro, P.; Rocco, G. P.; Salvato, B. *Arch. Biochem. Biophys.* **1994**, *313*, 318−327.

Scheme 4

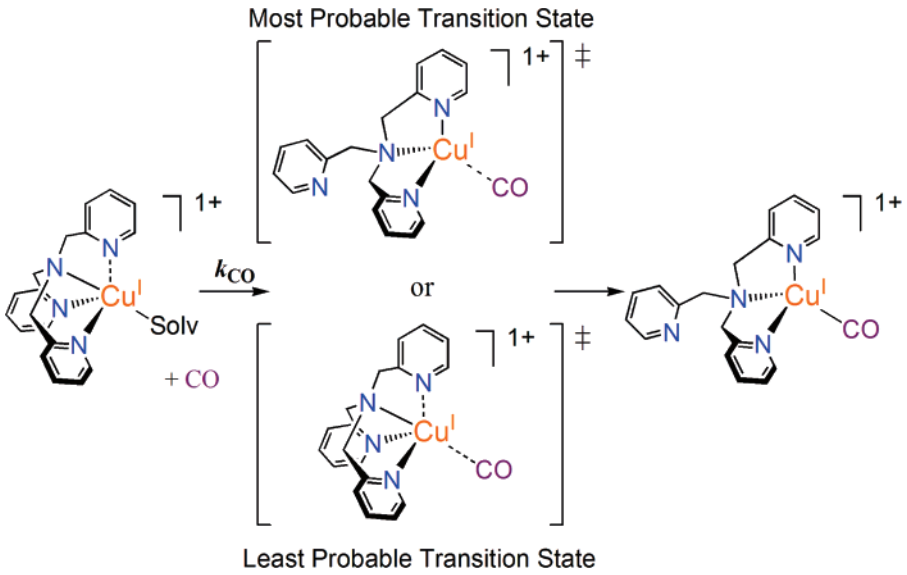

that closely resembles the final carbonylated product (i.e., a late transition state, Scheme 4). Even though the solvent interacts with the metal center, the reaction observed simply follows two reactants (copper complex and CO), forming one product (copper terminal carbonyl complex), which as expected yields a negative activation entropy. Negative entropic values are often identified as associative-type mechanisms. However, it would be premature to assign associative or dissociative mechanisms to CO coordination because the observed bimolecular rate constants are complicated by competitive solvent interactions with the cuprous center, which induces dissociation of ligand pyridyl arms. Yet, changing from coordinating (CH_3CN) to weakly coordinating (THF) solvent alleviates the competition between the solvent and CO, as indicated by the large drop in the $\Delta H^{\ddagger}$ terms for $\mathbf{1^H}$ and $\mathbf{3^{bqpa}}$. We suggest that if an even-less-coordinating solvent than THF was employed, $\Delta H^{\ddagger}$ may continue to decrease and the rate constant (k_{CO}) may continue to increase.

Determination of k_{-CO} (s^{-1}) and Corresponding Activation Parameters. From the experimentally derived k_{CO} and K_{CO} values, the CO dissociation rate constant k_{-CO} (s^{-1}), and its corresponding activation parameters can be calculated, (eq 1, Experimental Section). Collected data support a simple mechanism for CO de-ligation (i.e., the k_{-CO} process) from $[(L)Cu^{I}(CO)]^{+}$ complexes (Scheme 1). Within the R−TMPA series $\mathbf{1^R}$, the rate constant for CO dissociation ($k_{-CO} = 1.79 \times 10^4\ s^{-1}$) is smallest for the most thermodynamically stable complex, $[Cu^{I}(NMe_2\text{-tmpa})(CO)]^{+}$ ($\mathbf{1^{Me2N}}$**−CO**) in CH_3CN (Table 3). As the ligand becomes less electron donating from NMe_2− to MeO− to H−, the rate constant (k_{-CO}) becomes progressively larger. Thus, breakage of the Cu−CO bond is more difficult for the more-stable $\mathbf{1^{Me2N}}$**−CO** when compared to that for $[Cu^{I}(MeO\text{-tmpa})(CO)]^{+}$ ($\mathbf{1^{MeO}}$**−CO**) and $[Cu^{I}(tmpa)(CO)]^{+}$ ($\mathbf{1^{H}}$**−CO**). Further, the difficulty in breaking the Cu−CO bond (k_{-CO}) is evident by the very large $\Delta H^{\ddagger}$ terms for $\mathbf{1^{MeO}}$**−CO** (60.7 kJ mol^{-1}) and $\mathbf{1^{H}}$**−CO** (43.6 kJ mol^{-1}) in CH_3CN.

$\mathbf{3^{bqpa}}$**−CO** has the smallest off-rate of all of the compounds studied in CH_3CN, $k_{-CO} = 6.97 \times 10^3\ s^{-1}$, $\Delta H^{\ddagger}$, 49.6 kJ mol^{-1}. We presume the low off-rate is due to the steric hindrance of the bulky BQPA ligand, as the overall K_{CO} for $\mathbf{3^{bqpa}}$**−CO** formation is lower than the R−TMPA complexes $\mathbf{1^{H}}$**−CO** and $\mathbf{1^{MeO}}$**−CO**. The greatest contribution to the overall activation energy comes from the large $\Delta H^{\ddagger}$ term obtained for both $\mathbf{1^{H}}$**−CO** and $\mathbf{3^{bqpa}}$**−CO**. The $\Delta S^{\ddagger}$ term for these compounds is virtually 0 J $mol^{-1}\ K^{-1}$, suggesting a very small overall change from the coordinated carbonyl complex to the transition state (i.e., an early transition state, Scheme 4). In sharp contrast to the forward reaction (k_{CO}), $\Delta H^{\ddagger}$ for the reverse reaction (k_{-CO}) shows no dependence on solvent. The relatively large $\Delta H^{\ddagger}$ value corresponds directly to the simple weakening and breaking of the Cu−CO bond. Thus, the transition state for the simple dissociation of CO from $[(L)Cu^{I}(CO)]^{+}$ complexes resembles the terminal carbonyl complex (the converse being a late transition state for the forward reaction, CO binding to $[(L)Cu^{I}]^{+}$), where the solvent has no effect on the reaction (Scheme 4).

Summary of Kinetic Data and Activation Parameters. Through transient absorbance laser flash photolysis, the rate of CO association (k_{CO}) and dissociation (k_{-CO}) from copper(I) upon photodissociation has been quantified, along with the activation parameters that govern this process. As the electron-donating ability of the ligand increases such as in $\mathbf{1^R}$, the CO-binding rate (k_{CO}) increases and the CO dissociation rate (k_{-CO}) decreases. In a less-coordinating solvent, the decreased enthalpic barrier ($\Delta H^{\ddagger}$) for k_{CO} indicates that de-ligation of CH_3CN preceeds CO rebinding. Activation entropies ($\Delta S^{\ddagger}$) for k_{CO} indicate a late transition state, as supported by the activation parameters ($\Delta H^{\ddagger}$, $\Delta S^{\ddagger}$) for k_{-CO}. The inability to dissociate CO from $\mathbf{2^R}$ suggests that a strict N_3-coodination mode also only possessing five-membered chelate rings is necessary for photodissociation. The bulky quinolyl arms of BQPA that induce the desirable N_3-coodination mode in $\mathbf{3^{bqpa}}$ support this conclusion through a lower k_{CO} activation enthalpy ($\Delta H^{\ddagger}$) in comparison to $\mathbf{1^H}$.

Scheme 5

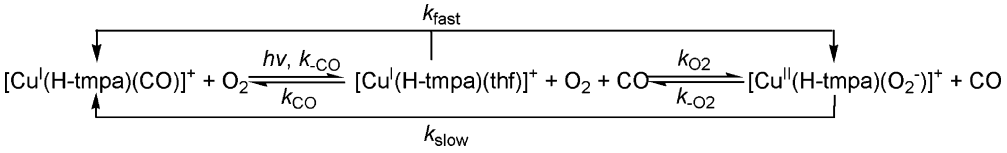

Table 4. Comparison of O_2 and CO Rate and Binding Constants at 298 K for $[Cu^{I}(H\text{-tmpa})(Solvent)]^{+}$ (**1^{H}**), Hemocyanin (Hc), and Selected Hemes

compound	K_{CO} (M^{-1})	K_{O2} (M^{-1})	k_{CO} (M^{-1} s^{-1})	k_{O2} (M^{-1} s^{-1})	k_{-CO} (s^{-1})	k_{-O2} (s^{-1})
$[Cu^{I}(H-tmpa)(THF)]^{+}$ (**1^{H}−CO**)	1.25×10^{5}	15.4	1.9×10^{9}	1.3×10^{9}	1.54×10^{4}	1.3×10^{8}
$[Cu^{I}(H-tmpa)(CH_3CN)]^{+}$ (**1^{H}−CO**)	220	0.38	5.9×10^{7}	5.8×10^{7}	2.68×10^{5}	1.5×10^{8}
hemocyanin (Hc)[7]	$(0.27 - 22) \times 10^{4}$	$(0.18 - 90) \times 10^{5}$	$(2.0 - 7.7) \times 10^{5}$	$(1.1 - 154) \times 10^{6}$	3−75	2.4 − 11.5
Fe(PF3CUIm) [a,40]	2.07×10^{9}	6.7×10^{4}	2.9×10^{7}	2.6×10^{8}	0.014	3.9×10^{3}
Fe(PF3CUPy) [a,40]	1.45×10^{8}	1.6×10^{3}	4.8×10^{7}	3.0×10^{8}	0.33	1.9×10^{5}
myoglobin − human (Mb) [39]	2.6×10^{7}	$(0.74 - 117) \times 10^{4}$	7.6×10^{5}	$(1.4 - 25) \times 10^{7}$	0.022	22
Hemoglobin − human, R state (Hb) [39]	4.6×10^{8}	$(2.87 - 47.6) \times 10^{5}$	4.6×10^{6}	$(2.9 - 22) \times 10^{7}$	0.009	13.1

[a] Fe(PF3CUIm) = *meso*-5α,10α,15α-tris(*o*-pivalamidophenyl)-20β-{*o*-{[3-(*N*-imidazolyl)propyl] ureido}phenyl}porphyrinatoiron; Fe(PF3CUPy) = *meso*-5α,10α,15α-tris(*o*-pivalamidophenyl)- 20β-{*o*-{[3-(3-pyridyl)propyl]ureido}phenyl}porphyrinatoiron.

Photodissociation of Small Molecules from Copper Proteins. As stated, the measurement of small molecule (CO, O_2, or NO) recombination rates via photolytic methods is a novel process for synthetic and biological copper(I) complexes. However, work by Gorren et al. indicated that photolysis of the nitrogen monoxide (NO) adduct of the type-1 blue copper protein, azurin (Az), resulted in photodissociation.[77] Formation of AzNO led to the disappearance of the $g = 2$ EPR signal and the signature 625 nm absorbance band. Upon photolysis, the original absorbance band reappears but not the EPR signal, leading to the suggestion that a photolabile $Cu^{I}-NO^{+}$ species was formed. Further investigation by Ehrenstein et al. involving temperature dependence of this process found that binding of NO to azurin is similar in nature to CO rebinding to myoglobin.[78] At temperatures less than 200 K, NO did not fully dissociate from AzNO upon photolysis, resulting in geminate recombination. Above 200 K, internal rebinding ceases as protein fluctuations become fast, resulting in NO escaping the protein matrix. In addition, such fluctuations decreased the internal barrier for ligand rebinding, leading to exponential binding of NO from the solvent. In contrast to Gorren et al., Ehrenstein and co-workers suggest that the photolabile species was a tetragonal $Cu^{II}-NO$ complex due to the growth of a new absorption band below 400 nm upon binding NO.

Photodissociation of O_2 has been recently observed for oxytyrosinase (Tyr_{oxy})[79] and oxyhemocyanin (Hc_{oxy}).[80] Hirota et al. report that 355 nm pulse irradiation of Tyr_{oxy} leads to the bleaching of the 345 nm absorbance band on a microsecond time scale, attributed to the dissociation of O_2 from the $\mu-\eta^2:\eta^2$-peroxodicopper(II) center.[79] Intensity recovery corresponding to the rebinding of O_2 to the deoxy enzyme occurs on a millisecond time scale. Geminate recombination of O_2 was not observed for Tyr but was observed on a 80 ps time scale for Hc by Floyd et al.[80] It is important to note that the likely primary interaction of the protein dicopper(I) site and dioxygen (i.e, formation of a $Cu-O_2\cdots Cu^{I}$ species) was never observed, reiterating the significance of gaining new insights of copper(I) interactions with small molecules through kinetic and thermodynamic analyses of well-defined coordination complexes.

Comparison of CO and O_2 Binding to Copper Complexes, Hemocyanin, and Hemes. Previously, we utilized the ability to photodissociate CO from **1^{H}−CO** to determine the rate of O_2-binding to **1^{H}** (Scheme 5).[38] In the present investigation, CO-binding to copper(I) complexes were studied as a redox-inactive surrogate. We find that CO indeed acts as an excellent O_2 surrogate because the results with regard to solvent interaction are nearly identical.[38,42] For both CO and O_2 binding to **1^{H}**, the enthalpy of activation ($\Delta H^{\ddagger}$) is significantly lowered in THF when compared to that of an organonitrile solvent. The off-rate of the small molecule ($Cu-CO$ or $Cu-O_2$ bond cleavage) is unaffected by the coordinating ability of the solvent, indicative of a dissociative mechanism. Of greater interest is the nearly identical rate constants obtained for the fast room-temperature binding of O_2 (k_{O2} (THF) = 1.3×10^{9} M^{-1} s^{-1} extrapolated from the low-temperature data) and CO (k_{CO} (THF) = 1.9×10^{9} M^{-1} s^{-1}, actual data obtained at room temperature) in the two solvents (Table 4).[38,42] However, the off-rate for O_2 release from $[Cu^{II}(tmpa)(O_2^{-})]^{+}$ ($k_{-O2} = 1.3 \times 10^{8}$ s^{-1}) in THF is significantly greater than that for CO due to the large, unfavorable entropy of activation term ($\Delta S^{\ddagger} = 105$ J mol^{-1} K^{-1} for the O_2 reaction,[38] compared to −0.7 J mol^{-1} K^{-1} for CO, Table 3) that most likely arises from the overall change in geometry; loss of CO $[Cu^{I}(tmpa)(CO)]^{+}$ to give $[Cu^{I}(tmpa)(thf)]^{+}$ involves re-ligation of the dangling pyridyl arm (Scheme 2). Overall, CO-binding to copper(I) is highly thermodynamically favored compared to O_2 (Table 4) but with respect to kinetics, the two small molecules appear to be nearly identical. This explains why in our previous study we observed highly competitive binding of CO and O_2 to **1^{H}**, with the overall thermodynamics favoring **1^{H}−CO**; in

(77) Gorren, A. C. F.; Deboer, E.; Wever, R. *Biochim. Biophys. Acta* **1987**, *916*, 38−47.
(78) Ehrenstein, D.; Nienhaus, G. U. *Proc. Natl. Acad. Sci. U.S.A.* **1992**, *89*, 9681−9685.
(79) Hirota, S.; Kawahara, T.; Lonardi, E.; deWaal, E.; Funasaki, N.; Canters, G. W. *J. Am. Chem. Soc.* **2005**, *127*, 17966−17967.
(80) Floyd, J. S.; Haralampus-Grynaviski, N.; Ye, T.; Zheng, B.; Simon, J. D.; Edington, M. D. *J. Phys. Chem. B* **2001**, *105*, 1478−1483.

the presence of CO, $[Cu^{II}(tmpa)(O_2^-)]^+$ equilibrates back to $[Cu^{I}(tmpa)(CO)]^+$, allowing the determination of k_{slow} (Scheme 5).[38]

Carbon monoxide binding constants (K_{CO}) for the dicopper(I) site in hemocyanin (Hc)[7] are comparable to that reported here for mononuclear copper complexes, Table 4. However, O_2-binding is significantly enhanced ($>10^4$ M^{-1}) in the case of Hc and can easily be attributed to the dicopper center of Hc stabilizing the dioxygen adduct, a peroxo dicopper(II) complex where *both* copper ions are involved; CO only binds to one of the copper centers.[9,81−85] Thus, comparisons of CO-binding to these copper complexes and Hc are more relevant than O_2-binding. The rate at which CO binds to copper is greatly enhanced in the case of our copper complexes versus Hc (Table 4). These k_{CO} values are however affected by several factors including but not limited to redox potentials and the ligand/protein environment. Yet, they also exhibit greater rates of CO dissociation (k_{-CO}) than those exhibited by Hc. The higher dissociation rates for both CO and O_2 from these copper(I) complexes in comparison to copper and heme proteins (Table 4 and discussion above) are not only due to the more energy needed to break the protein ligand−metal bond but also are due to the greater complexity of the protein matrix.

Heme proteins and model systems have been studied extensively and commonly employ carbon monoxide as a redox-inactive surrogate to dioxygen.[28−30,34,35,39−41,86,87] The results presented here showing that copper rapidly reacts with both CO and O_2 are in line with studies carried out on synthetic heme species. However, the copper(I) complexes bind dioxygen and carbon monoxide at a much faster rate than hemes but not with as high of an affinity. This phenomenon is relevant to the mechanism of ligand exchange in C*c*O, displaying that Cu_B plays a regulatory role in the kinetics of binding small molecules to the C*c*O heme/copper active site.[28−30,86,87] The first synthetic model system, $[(^6L)Fe^{II}(CO)\cdots Cu^{I}]^+$, directed at mimicking the CO transfer chemistry of the $heme_{a3}/Cu_B$ active site of C*c*O was reported from our lab.[88] This binucleating ligand system (^6L) is composed of a tetradentate chelate for copper (analogous to $\mathbf{1^H}$) covalently appended to the periphery of a difluorophenyl-substituted porphyrinate. Like C*c*O, photodissociation of CO from $[(^6L)Fe^{II}(CO)\cdots Cu^{I}]^+$ results in the initial transfer of CO to the copper(I) moiety forming $[(^6L)Fe^{II}\cdots Cu^{I}(CO)]^+$ before thermally equilibrating back to the initial species.[88]

Summary/Conclusions. In previous work, the ability to photodissociate carbon monoxide from $[Cu^{I}(tmpa)(CO)]^+$ ($\mathbf{1^H-CO}$) via MLCT ($Cu^{I}(d_{10})-N_{py}(\pi^*)$) excitation was established.[38] Now, the properties that govern this process have been systematically investigated through the variation of the ligand environment around the copper(I) metal center. Characterization of the carbonyl adducts of **1**−**3** was accomplished via X-ray crystallographic studies, cyclic voltammetry, along with infrared (solid and solution) and UV−vis spectroscopies. In addition, various experimental techniques were utilized to determine equilibrium binding constants (K_{CO}), association (k_{CO}) and dissociation (k_{-CO}) rate constants, as well as the thermodynamic ($\Delta H°$, $\Delta S°$) and activation parameters ($\Delta H^‡$, $\Delta S^‡$) that regulate this process.

First, a group of tetradentate ligand copper−CO species (Chart 1) were structurally characterized. Through solid and solution analyses, it was determined that the photolabile carbonyl species in solution possesses a tridentate coordination mode to the copper ion with one dangling arm of the tripodal ligand.

Second, it was elucidated how ligand electronic effects and geometry dictate the strength in which CO binds to the cuprous metal. When the electron-donating ability of the tripodal, tetradentate ligand is increased, greater π back-bonding results in stronger Cu−CO bonds, leading to K_{CO} values on the order $\mathbf{1^{Me2N}-CO} > \mathbf{1^{MeO}-CO} > \mathbf{1^{H}-CO}$. With systematic synthetic expansion of the five-membered chelate rings like $\mathbf{1^R}$ to six-membered chelate rings like $\mathbf{2^R}$, the stability of the CO adduct decreases, $\mathbf{1^H-CO} > \mathbf{2^{pmea}-CO} > \mathbf{2^{pmap}-CO}$. Because of the more-favorable tetrahedral ligation of the PMEA and PMAP ligands to the copper alone, $\mathbf{2^R}$ are less reactive as reflected by their increased $E_{1/2}$ values. $\mathbf{3^{bqpa}}$ did not follow any trends because of its bulkier ligand framework, which consistently favors an N_3 coordination mode. By contrast, $\mathbf{1^R}-\mathbf{2^R}$ exhibit both N_3 and N_4 coordination modes in the absence of CO.

Third, CO photodissociated from $\mathbf{1^{Me2N}-CO}$, $\mathbf{1^{MeO}-CO}$, $\mathbf{1^{H}-CO}$, and $\mathbf{3^{bqpa}-CO}$ in coordinating (CH_3CN) and weakly coordinating (THF) solvent but not from $\mathbf{2^{pmea}-CO}$ and $\mathbf{2^{pmap}-CO}$. Each of the compounds that displayed CO photodissociation behavior possess an N_3 coordination mode forming strictly five-membered chelate rings. In CH_3CN, no particular trend in relation to the ligand environment was observed when following the post-photolytic bimolecular recombination of CO (k_{CO}) to the cuprous metal, where CO + $\mathbf{1^{Me2N}} > \mathbf{1^{H}} > \mathbf{1^{MeO}} > \mathbf{3^{bqpa}}$. In THF, bimolecular recombination was observed where CO + $\mathbf{1^{H}} > \mathbf{3^{bqpa}}$.

Finally, values for the dissociation of CO from copper(I)−CO complexes ($k_{-CO} = k_{CO}/K_{CO}$) were derived with a clear trend with respect to electron-donating ability, where k_{-CO} for $\mathbf{1^{Me2N}-CO} < \mathbf{1^{MeO}-CO} < \mathbf{1^{H}-CO}$. This simply means that the terminal carbonyl complexes are more favored, that is, the equilibrium lies to the left, as CO-release becomes increasingly more difficult with greater ligand electron-donating ability, resulting in stronger Cu−CO complexes.

These findings offer clues as to how CO photodissociates from $[(L)Cu^{I}(CO)]^+$ complexes and how copper binds small molecules (CO and O_2) in relation to other biologically relevant copper complexes as well as proteins. Such insights

(81) Root, R. W. *J. Biol. Chem.* **1934**, *104*, 239−244.
(82) Peisach, J.; Aisen, P.; Blumberg, W. E. *The Biochemistry of Copper*; Academic Press: New York, 1966.
(83) Fager, L. Y.; Alben, J. O. *Biochemistry* **1972**, *11*, 4786.
(84) Connelly, P. R.; Gill, S. J.; Miller, K. I.; Zhou, G.; Vanholde, K. E. *Biochemistry* **1989**, *28*, 1835−1843.
(85) Connelly, P. R.; Johnson, C. R.; Robert, C. H.; Bak, H. J.; Gill, S. J. *J. Mol. Biol.* **1989**, *207*, 829−832.
(86) Fiamingo, F. G.; Altschuld, R. A.; Moh, P. P.; Alben, J. O. *J. Biol. Chem.* **1982**, *257*, 1639−1650.
(87) Dyer, R. B.; Einarsdottir, O.; Killough, P. M.; Lopezgarriga, J. J.; Woodruff, W. H. *J. Am. Chem. Soc.* **1989**, *111*, 7657−7659.
(88) Fry, H. C.; Cohen, A. D.; Toscano, J. P.; Meyer, G. J.; Karlin, K. D. *J. Am. Chem. Soc.* **2005**, *127*, 6225−6230.

include the possible transient binding of small molecules to the Cu_B active site of C*c*O prior to binding to the $heme_{a3}$ active site. Carbon monoxide binds faster to these copper(I) complexes than most hemes, but thermodynamics favor heme−CO species.

Acknowledgment. We are very grateful for financial support of this research (K.D.K., National Institutes of Health, Grant GM28962; G.J.M., National Science Foundation, Grant CHE 0616500).

Supporting Information Available: Additional cyclic voltammetry, infrared spectra, ^{1}H NMR spectra, spectrophotometric titrations, Van't Hoff plots, transient absorption difference spectra, linear [CO] dependence, Eyring plots, crystal structures and CIF files for crystal structures. This material is available free of charge via the Internet at http://pubs.acs.org.

IC701903H